JOURNAL OF PETROLOGY | VOLUME 55 | NUMBER 10 | PAGES 2067–2096 | 2014 | doi:10.1093/petrology/egu050

Experimental Study of the Influence of Water on Melting and Phase Assemblages in the Upper Mantle

DAVID H. GREEN[1,2]*, WILLIAM O. HIBBERSON[2], ANJA ROSENTHAL[2,3], ISTVÁN KOVÁCS[2,4], GREGORY M. YAXLEY[2], TREVOR J. FALLOON[5] AND FRANK BRINK[6]

[1]SCHOOL OF EARTH SCIENCES AND CENTRE FOR ORE DEPOSIT STUDIES, UNIVERSITY OF TASMANIA, HOBART, TAS 7001, AUSTRALIA

[2]RESEARCH SCHOOL OF EARTH SCIENCES, AUSTRALIAN NATIONAL UNIVERSITY, CANBERRA, ACT 0200, AUSTRALIA

[3]BAYERISCHES GEOINSTITUT, UNIVERSITY OF BAYREUTH, 95440 BAYREUTH, GERMANY

[4]GEOLOGICAL AND GEOPHYSICAL INSTITUTE OF HUNGARY, LABORATORY DEPARTMENT, BUDAPEST, STEFÁNIA ÚT U. 43, H-1143, HUNGARY

[5]SCHOOL OF EARTH SCIENCES AND INSTITUTE FOR MARINE AND ANTARCTIC STUDIES, UNIVERSITY OF TASMANIA, HOBART, TAS 7001, AUSTRALIA

[6]CENTRE FOR ADVANCED MICROSCOPY, AUSTRALIAN NATIONAL UNIVERSITY, CANBERRA, ACT 0200, AUSTRALIA

RECEIVED OCTOBER 21, 2013; ACCEPTED AUGUST 21, 2014

The role of water in the uppermost mantle has been explored to 6 GPa (~200 km) by a novel experimental approach in which the silicate melting solidus, the stability of hydrous phases and the H_2O contents in nominally anhydrous minerals (NAMs) were determined. The composition studied is a fertile lherzolite modelled as a source for mid-ocean ridge basalts (MORB). The use of crushed olivine as traps for melt or fluid inclusions allows a distinction to be made between quenched hydrous silicate melt and quench material from water-rich vapour phase. The vapor-saturated solidus (water-rich vapor) of fertile lherzolite increases in temperature (T) from a minimum of 970°C at 1·5 GPa (~50 km) to 1375°C at 6 GPa. The Ca-rich amphibole pargasite is stable to the vapour-saturated solidus to 3 GPa (~100 km). Based on normative components, at 2·5 GPa the near-solidus melt (1–2%) in mantle with very low H_2O content is transitional between sodic–dolomitic carbonatite and olivine melilitite. With higher melt fraction (~5%) at higher T or higher H_2O content it is olivine-rich basanite. Both immediately below and above the solidus, the H_2O content in residual lherzolite is ~200 ppm retained in NAMs at 2·5 and 4 GPa. The experimentally determined vapour-saturated solidus corrects recent numerical models of melting of lherzolite + H_2O based on inferred high solubilities of H_2O in NAMs and accounts for a discrepant experimental determination of the vapour-saturated solidus in which very high water/rock ratios were used. At 2·5 ± 0·1 GPa, the water content of experimental charges was varied from 0·05 to 14·5 wt %. Below the solidus and with increasing water content from 0·05 to 2·9 wt %, pargasite decreases in K_2O and Na_2O content and is absent in experiments with 7·25 and 14·5 wt % H_2O. Also with increasing water content from 0·05 to 14·5 wt % H_2O, the Na_2O content of clinopyroxene decreases from 1·6 wt % to below the limit of detection (0·2 wt %). The destabilization of pargasite and change of clinopyroxene composition at 2·5 GPa and 1000°C are attributed to the leaching role (Na_2O and K_2O particularly) of the water-rich vapour at high water/rock ratios. The hydrous mineral pargasite is the major site of H_2O storage in fertile uppermost mantle lherzolite but pargasite is unstable at pressures (P) >3 GPa (~100 km depth), causing a sharp drop in the water storage capacity of the upper mantle from >2000 to ~200 ppm. For small H_2O contents (<2000 ppm approximately), the temperature of the vapour-undersaturated solidus of fertile upper mantle lherzolite decreases

*Corresponding author. Telephone: +61 3 6226 2814 (work), +61 3 6225 0430 (home), +61 4 0800 5538 (mobile). Fax: +61 3 6226 2547. E-mail: david.h.green@utas.edu.au

sharply with increasing P *at ~90 km depth. The negative d*T*/d*P *for the vapour-undersaturated solidus has important rheological and geodynamic consequences. In oceanic intraplate settings, the geotherm passes from subsolidus pargasite-bearing lherzolite to garnet lherzolite with incipient melting, creating the rheological boundary at ~90 km depth, between lithosphere and asthenosphere. The asthenosphere becomes geochemically zoned with the 'enriched' intraplate basalt source (>500 ppm H_2O) overlying the 'depleted' MORB source (~200 ppm H_2O) in the deeper asthenosphere. Water also plays a significant role at convergent margins, where hydrous silicate melting in the mantle wedge is initiated at the vapour-saturated solidus. Melting of lherzolite at or near the vapour-saturated solidus does not fully dehydrate residual lherzolite or harzburgite. Residual lithosphere returned to the upper mantle may carry ~100–200 ppm H_2O. At 6 GPa the low K/Na model mantle composition (MORB-source mantle) with >200 ppm H_2O has normal rather than supercritical melting behaviour with the solidus at 1375°C, which is ~350°C below the C + H-free solidus.*

KEY WORDS: *experimental petrology; hydrous mineral phases pargasite and phlogopite; nominally anhydrous minerals; upper mantle melting; water in the upper mantle, lithosphere, asthenosphere*

INTRODUCTION

The presence of water in the Earth's interior has a major effect on the temperature (T) of melting of the upper mantle and on the melt fraction formed. Water is a trace component in mid-ocean ridge basalt (MORB) magmas and a minor component in primitive intraplate and island arc magmas. Water is present in hydrous minerals such as amphibole, mica, chlorite or serpentine, which may be stable at or below the solidi of mantle compositions. The phase relationships and particularly the solidus of hydrous upper mantle must be determined experimentally, and controversy has arisen between experimental studies advocating very low solidus temperatures (~810°C) from 2 to 6 GPa (Mysen & Boettcher, 1975; Grove *et al.*, 2006; Till *et al.*, 2012a, b) or much higher T and positive dT/dP from ~975°C at 1·5 GPa to 1375°C at 6 GPa (Kushiro *et al.*, 1968; Green, 1973*a*; Millhollen *et al.*, 1974; Green *et al.*, 2010, 2011; Tumiati *et al.*, 2013) (see Supplementary Data Electronic Appendix EA 1 'Previous work'; supplementary data are available for downloading at http://www.petrology.oxfordjournals.org).

Also, water is a trace component in nominally anhydrous minerals (NAMs), including olivine and pyroxenes, and a major role has been proposed for water in affecting the rheology of the upper mantle. Hirth & Kohlstedt (1996) argued that dilute solid solution of intracrystalline water in NAMs has a marked weakening effect on crystal structure and lowers effective viscosity in the upper mantle. They suggested that the mantle part of the lithosphere is 'dry' residual peridotite after melt extraction has removed water from NAMs, whereas the underlying asthenosphere, having not experienced upwelling and melt extraction, is interpreted as having lower viscosity owing to water retained in NAMs. A recent study by Fei *et al.* (2013) argued that water in mineral structures has little effect on upper-mantle rheology, based on silicon self-diffusion coefficients in single-crystal forsterite. In addition, Girard *et al.* (2013) also proposed that the presence of free fluid or melt plays a more important role than the water content of NAMs in controlling the rheology of the upper mantle. A petrology-based model (Green, 1971; Green *et al.*, 2010; Kovács *et al.*, 2012) suggests that the stability of the amphibole pargasite at <3 GPa provides higher water storage capacity in crystal sites. However, at >3 GPa pargasite is not stable and small quantities of water exceed that stored in NAMs, thus lowering solidus temperatures and producing interstitial melting controlled by water content (incipient melting) (Lambert & Wyllie, 1970; Green, 1971; Green & Falloon, 1998, 2005; Green *et al.*, 2010). In this model the intraplate geotherm enters a region of incipient melting at ~3 GPa—the asthenosphere—and traverses this interval of incipient melting to re-enter the subsolidus region at depth. The second intersection of geotherm and solidus is a consequence of the positive dT/dP of the vapour-saturated solidus at >2 GPa, leading to high solidus temperature at 6 GPa. This would not happen if the solidus remained at <850°C at 2–6 GPa (Grove *et al.*, 2006; Till *et al.*, 2012*a*). In commenting on the disagreement on the solidus temperature of lherzolite with water-rich vapour, Foley (2011) emphasized the role of high-silicate solute in lowering water activity in the vapour phase, at high pressure particularly, and thus increasing the solidus temperature. Lowering of the water activity in a vapour phase by increased solute in the vapour has also been advocated by Green *et al.* (2010), Ardia *et al.* (2012), Kovács *et al.* (2012) and Gaetani *et al.* (2014), and reflects partitioning of components between vapour and equilibrium minerals (and melt where present). The effect is applicable to all lherzolites and cannot account for differences of 200–500°C between solidus temperatures inferred in studies on similar lherzolite compositions and water/rock ratios at the same P–T conditions. Our study was designed to resolve these mutually incompatible interpretations of very similar experiments.

In the recent work of Grove *et al.* (2006) and Till *et al.* (2012*a*), additional important differences from earlier studies are the identification of chlorite at and above the solidus from 2 to 5 GPa and the restriction of amphibole (pargasite) to pressures <2 GPa [compared with <3 GPa (Green, 1973*b*, 1976; Millhollen *et al.*, 1974; Mengel & Green, 1989; Wallace & Green, 1991; Niida & Green, 1999; Fumagalli *et al.*, 2009; Green *et al.*, 2010; Tumiati *et al.*, 2013)]. The differences in observation and interpretation of peridotite melting have significant importance for

geophysical, geodynamic and petrological modelling of upper mantle characteristics, including convergent margins, and suggest a need for reconciliation of the newer and earlier results.

EXPERIMENTAL STRATEGY

After confirming that we obtained run products analogous to those observed in several experiments at the same P–T conditions and water contents by Grove *et al.* (2006) (see Supplementary Data EA 1 and 2), we focused initial work at 2·5 GPa, 1000°C. We addressed the principal difference in method, the high water contents (14·5 wt %) used by Grove *et al.* (2006), by varying the water contents in our experimental charges from ~0·05 to 14·5 wt %. The chosen run conditions are ~150°C above the vapour-saturated lherzolite solidus inferred by Grove *et al.* (2006) but are just below the same solidus as inferred by others (Kushiro *et al.*, 1968; Green 1973*b*, 1976; Millhollen *et al.*, 1974; Mengel & Green, 1989; Niida & Green, 1999; Wallace & Green, 1991; Green *et al.*, 2010, 2011; Tumiati *et al.*, 2013). The P–T conditions are also outside the pargasite stability field found by Grove *et al.* (2006) and Till *et al.* (2012*a*), but within the pargasite stability field for lherzolite + H_2O found by others (Green, 1973*b*, 1976; Millhollen *et al.*, 1974; Mengel & Green, 1989; Wallace & Green, 1991; Niida & Green, 1999; Fumagalli *et al.*, 2009; Green *et al.*, 2010, 2011; Tumiati *et al.*, 2013). In the experiments at 2·5 GPa we also developed a complementary technique to the experimental study of phase relationships by including layers of crushed olivine at the top and bottom of the capsules. These layers acted as melt or vapour traps for the lherzolite under investigation, and were also analysed by Fourier transform infra-red (FTIR) spectroscopy to determine water contents in the nominally anhydrous olivine (Green *et al.*, 2010; Kovács *et al.*, 2012). Substituting orthopyroxene or clinopyroxene for olivine allowed measurement of partitioning of water between NAMs (i.e. olivine, clinopyroxene, orthopyroxene) at the P–T conditions and in the chemical system (fertile lherzolite) directly relevant to mantle melting, pargasite stability and vapour-saturation. Following the detailed study at 2·5 GPa, we determined the solidus temperatures at 4 and 6 GPa, in most cases with 1·45 or 0·145 wt % H_2O. The details of the FTIR aspect of the study have been presented by Kovács *et al.* (2012). A similar approach, also using lherzolite and olivine layers, was followed by Ardia *et al.* (2012).

Distinguishing between vapour-phase quench and quenched hydrous silicate melt

From the pioneering study of Bowen & Tuttle (1949) on MgO–SiO_2–H_2O, it has been known that aqueous vapour in the presence of olivine and orthopyroxene at high pressures dissolves significant amounts of SiO_2 and other oxides and that quenching of the vapour forms siliceous glass (Nakamura & Kushiro, 1974; Stalder *et al.*, 2001; Mibe *et al.*, 2002, 2007; Bali *et al.*, 2008). As a consequence, glass quenched from a high-pressure vapour phase has been described as yielding thin films, fragmented 'froth', filaments, tiny glass spheres in void space, and crystal coatings (Niida & Green, 1999; Mibe *et al.*, 2007; Green *et al.*, 2010, 2011). Rarely, investigators have inferred two coexisting fluid phases on the basis of observed wisps and filaments of glass with microlites of quench minerals (suggested as quenched from hydrous silicate melt), and films and spheres of glass (suggested as quenched from water-rich vapour) (Adam *et al.*, 1997; Till *et al.*, 2012*a*). Criteria must be sought to distinguish between glass quenched from an aqueous vapour phase, from a hydrous silicate melt, or from a supercritical fluid (Stalder, 2012).

The understanding of hydrous melting of the mantle also requires information on the liquidus temperatures and liquidus phases of water-saturated melts and the limits to water solubility in mantle-derived melts. Experimental studies (Green, 1973*a*; Nicholls & Ringwood, 1973; Green *et al.*, 1975; Edgar *et al.*, 1976; Brey & Green, 1977; Adam *et al.*, 1997; Falloon & Danyushevsky, 2000; Irving & Green, 2008) on basalts + H_2O at high pressure have defined an empirical relationship between liquidus depression and dissolved water content for olivine-rich melts (Fig. 1; also Falloon & Danyushevsky, 2000, fig. 8; Green *et al.*, 2001, fig. 2). Maximum water contents in olivine-rich basaltic melts at vapour-saturation are 25–30 wt % H_2O at 2·5–3 GPa and, importantly, glasses or quench phases from the liquid are relatively Fe-rich (Mg# = 75–80) with respect to coexisting olivine or pyroxenes (Mg# = 90–93) [Mg# is 100 Mg/(Mg + Fe)].

Based on these earlier studies, the presence within the lherzolite and 'melt-trap' layers of interstitial patches (interserts) of acicular or lath-shaped crystals of amphibole (and/or quench clinopyroxene), mica and glass, all with Mg# ~ 70–85 and commonly showing Fe/Mg zoning in laths, is evidence for quenched hydrous silicate melt (Fig. 2; Green *et al.*, 2010, supplementary fig. S2). Conversely, the absence of an intersertal texture with iron-enriched quench phases, together with the presence of porous texture, planes of fluid inclusions in olivine, and the stability of hydrous pargasite or phlogopite with Mg# similar to or greater than that of olivine, are indicators of subsolidus conditions and the presence of an aqueous vapour phase. As the vapour phase at subsolidus conditions contains dissolved oxides at high pressure, quenching produces glass as thin films, crystal coatings, fragmented 'froth' or glass spheres (Fig. 3).

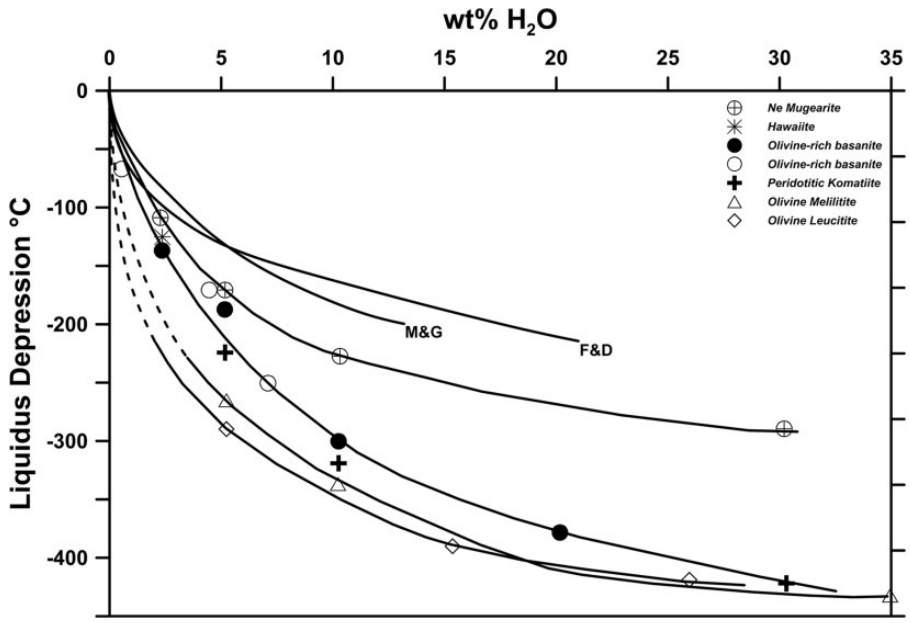

Fig. 1. Experimental determination of the liquidus depression in olivine-rich magmas as a function of dissolved water content at high pressure. Data from experimental studies in which the anhydrous and water-saturated liquidi have been determined at several pressures (Green, 1973*a*, Olivine-rich basanite; Green & Hibberson, 1970, hawaiite; Green *et al.*, 1975, peridotitic komatiite; Edgar *et al.*, 1976, Olivine leucitite; Brey & Green, 1977, Olivine melilitite; Falloon & Danyushevsky, 2000, F&D; Medard & Grove, 2008, M&G; Irving & Green, 2008, Nepheline mugearite).

EXPERIMENTAL AND ANALYTICAL METHODS

Preparation of starting materials

The composition HZ1 (Table 1) used is a model mantle composition (Hart & Zindler, 1986). Both HZ1 and the MOR Pyrolite composition are estimates of the source lherzolite for MORB, commonly equated with asthenospheric mantle composition. The compositions were prepared by sintering appropriate proportions of high-purity oxides (Si, Ti, Al) or carbonates (Ca, Na, K), then adding Fe as synthetic fayalite, and all Mg as fired MgO (dry mix) or $Mg(OH)_2$. Batches (2 g) were prepared of two HZ1 compositions differing only in water content, one anhydrous (mix A) and one with 14·5 wt % H_2O (mix B), as in the study by Grove *et al.* (2006). A second composition HZ2 (Table 1) [in both the anhydrous and hydrous (14·5 wt % H_2O) end-members] was used, which differed from HZ1 only in the addition of a lower amount of fayalite in the preparation steps (i.e. approximately half the FeO content of HZ1). Consequently, run products from HZ2 have higher Mg# in all phases (93–94 compared with 90–91 in olivine). As HZ1 and HZ2 have the same relative proportions of all oxides except Fe, any differences in phase assemblage (such as chlorite rather than pargasite or a higher solidus temperature) or in phase compositions, between HZ1 and HZ2 at the same P–T, may be attributed to higher Mg# (i.e. the more refractory nature of HZ2). A third composition (Table 1) enriched in K_2O and calculated as HZ1 +5 wt % anhydrous phlogopite was prepared as a sintered oxide mix and mixed with the HZ1 hydrous mix in 90:10 and 99:1 proportions to obtain K-enriched lherzolite with 1·45 and 0·145 wt % H_2O respectively. The purpose of the K-enriched composition was to briefly investigate the role of phlogopite as a hydrous phase stable to higher pressures than pargasite. The experiments on this composition are discussed in Supplementary Data EA 9.

The water content of 100 mg batches of these starting materials was controlled from 0·073 to 7·25 wt % by mixing A and B compositions in appropriate proportions. An alternative method of obtaining starting material with a fixed water content applied the results and methods of Niida & Green (1999) to prepare 100 mg samples of two pargasite-bearing lherzolites, synthesized from the HZ1 anhydrous composition at 1·5 GPa, 950°C (P77-2) and 3 GPa, 950°C (P77-1) by adding 1 and 0·5 wt % H_2O respectively by microsyringe. The synthesis experiments yielded spinel + pargasite lherzolite (P77-2) and pargasite + garnet lherzolite (P77-1). The added water contents are greater than that which can be accommodated in pargasite in the HZ1 composition at the synthesis conditions (see Niida & Green, 1999). Excess water was driven off by drying at 200°C. From the bulk composition and analyses of all phases, a mass-balance calculation yields 15 wt % pargasite (Supplementary Data EA 4; P77-2). Satisfactory analyses of pargasite were not obtained

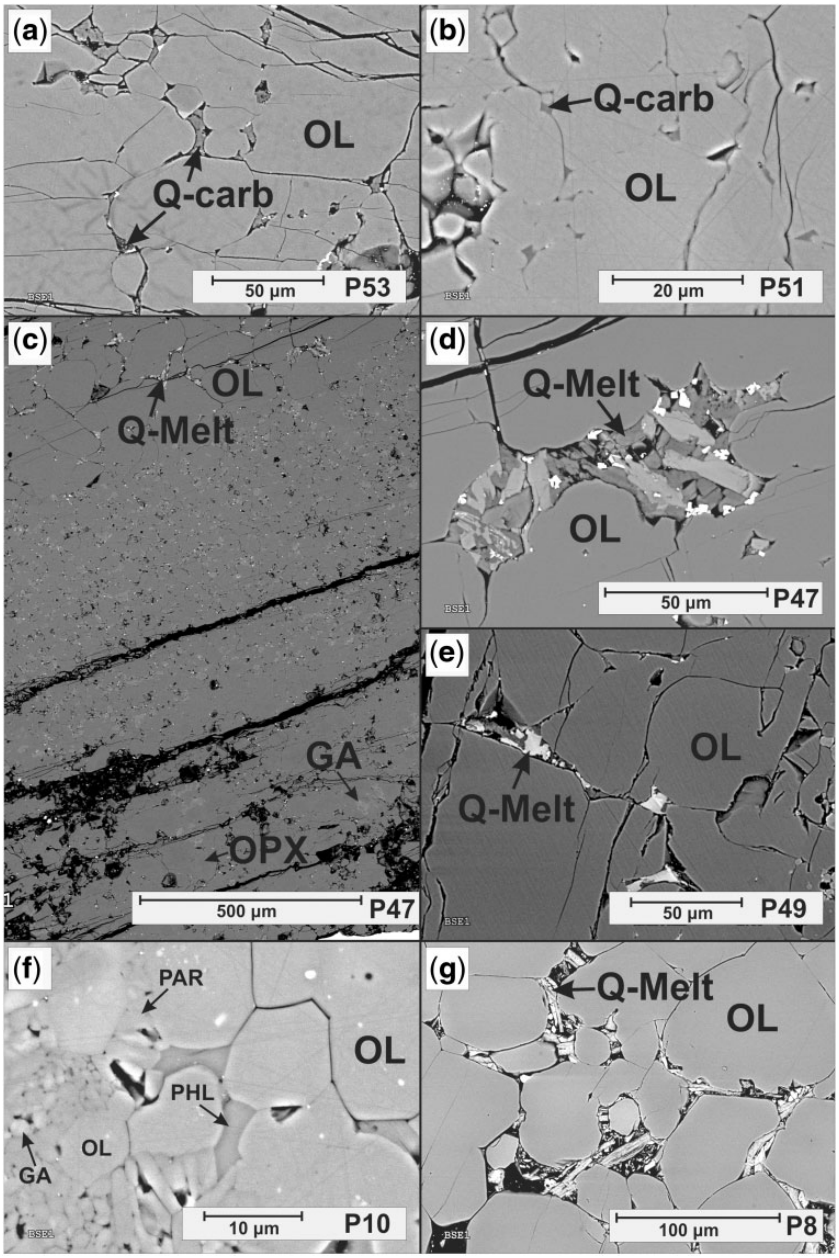

Fig. 2. SEM images illustrating experiments below and above the hydrous silicate melt solidus, particularly at 2·5 and 6 GPa. (a) P53, HZ1 at 6 GPa, 1300°C, 1·45 wt % H_2O. Image shows the olivine layer with a small amount of quench dolomitic carbonate (Q-carb) and oxide in interstices between olivine grains (Supplementary Data EA 3). (b) P51, HZ1 at 6 GPa, 1350°C, 0·145 wt % H_2O. Image shows the olivine layer with a very small amount of quench dolomitic carbonate in interstices between olivine grains (Supplementary Data EA 3). (c) P47, HZ1 at 6 GPa, 1400°C, 1·45 wt % H_2O. Image shows the three layers of the experimental charge. The upper olivine layer contains quenched hydrous, carbonate-bearing silicate melt in an intersertal texture between olivine crystals. The middle layer is garnet lherzolite and the lower layer is low-alumina orthopyroxene with minor Cr-rich garnet (GA) (Supplementary Data EA 3). The image illustrates the role of the olivine layer as a melt-trap for melt generated in the lherzolite layer and the re-equilibration of the initial orthopyroxene to lower Al content, with exsolved garnet. Both the olivine and orthopyroxene layers are designed for FTIR analyses (Kovács *et al.*, 2012). (d) P47, HZ1 at 6 GPa, 1400°C, 1·45 wt % H_2O. A higher magnification image of the olivine layer in (c) shows the quenched hydrous, carbonate-bearing silicate melt in an intersertal texture between olivine crystals. The quench phases include Fe-rich amphibole or clinopyroxene, dolomitic carbonate and titanomagnetite. There is also Fe-enrichment of olivine rims enclosing the melt intersert. (e) P49, HZ1 at 6 GPa, 1400°C, 1·45 wt % H_2O. A higher magnification image of the olivine layer shows the quenched hydrous, carbonate-bearing silicate melt in an intersertal texture between olivine crystals. (f) P10, HZ1 +5% anhydrous phlogopite at 2·5 GPa, 1000°C, 0·145 wt % H_2O. Boundary between phlogopite lherzolite and olivine layers. Subsolidus assemblage with magnesian phlogopite and pargasite (Table 2). (g) P8, HZ1 +5% anhydrous phlogopite at 4 GPa, 1150°C, 1·45 wt % H_2O. Olivine layer with intergranular hydrous and carbonate-bearing silicate melt. Quenched melt (Q-melt) contains Fe-rich biotite (Supplementary Data EA 3).

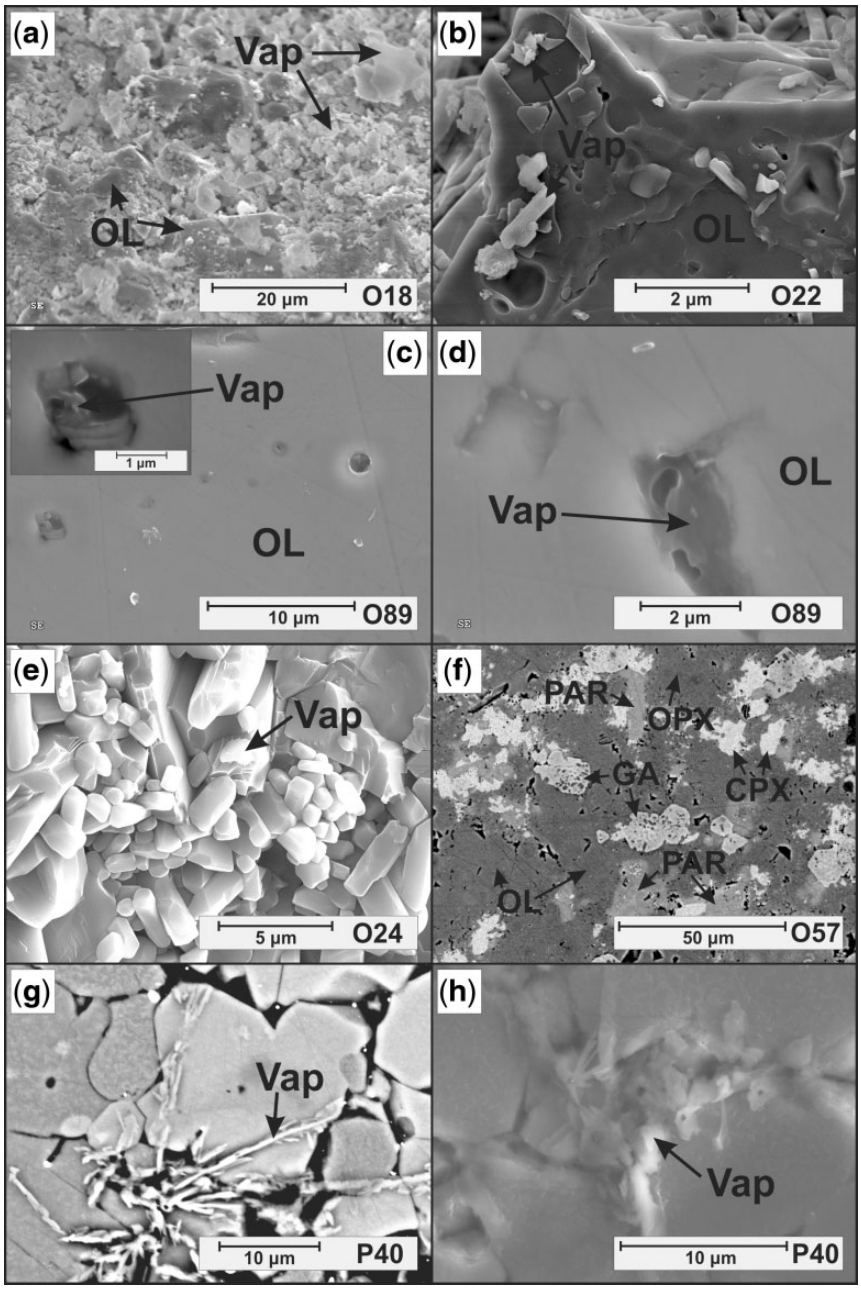

Fig. 3. Scanning electron microscope (SEM) images of experimental charges with vapour and vapour-phase quench. The images (a)–(f) of experimental runs are in the order of added water concentration from the highest wt % of added H_2O to lowest wt % of added H_2O. The images (g) and (h) are of the K-enriched HZ1 +5% anhydrous phlogopite composition at 6 GPa, 1200°C in which phlogopite does not appear and may be replaced by solute-rich fluid, now represented by fluid-phase quench. (a) O18 (O17), HZ2 at 2·4 GPa, 960°C, 14·5 wt % H_2O. Secondary electron image of broken surfaces of garnet lherzolite. Fragmented films of glass attached to euhedral olivine crystals and to capsule wall, interpreted as vapour-phase quench. In this experiment and that in (b), the experimental charge contained ~30 vol. % water-rich vapour before quenching. [See also fig. S1 (G) of Green *et al.* (2010).] (b) O22, HZ2 at 2·8 GPa, 840°C, 14·5 wt % H_2O. Secondary electron image of broken surfaces of garnet lherzolite. Thin 'skin' of glass draped over euhedral olivine crystals, interpreted as vapour-phase quench. [See also fig. S1 (H) of Green *et al.* (2010).] (c) O89, HZ2 at 2·5 GPa, 1000°C, 7·25 wt % H_2O. Back-scattered electron image of garnet lherzolite. Linear array of fluid inclusions on healed fracture in olivine disc. Some inclusions contain vapour-phase quench (see inset). (d) O89, HZ2 at 2·5 GPa, 1000°C, 7·25 wt % H_2O. Secondary electron image of quenched glass within fluid inclusion trapped in olivine disc. (e) O24, HZ2 at 2·4 GPa, 960°C, 1·45 wt % H_2O. Secondary electron image of broken surfaces of pargasite garnet lherzolite. Euhedral phases separated by pores (vapour phase) with uncommon small glass filaments. This experiment contained ~3 vol. % water-rich vapour before quenching [compare with (a) and (b)]. (f) O57, HZ2 at 2·5 GPa, 1000°C, 0·073 wt % H_2O. Back-scattered electron image of pargasite-bearing garnet lherzolite. Olivine, orthopyroxene, clinopyroxene, garnet and pargasite in intergrowth with very low porosity. The order of decreasing 'brightness' in the images is clinopyroxene > garnet (poikilitic) > pargasite > olivine > orthopyroxene. [See also fig. S1 A and B of Green *et al.* (2010).] (g) P40, HZ2 +5% anhydrous phlogopite at 6 GPa, 1200°C, 0·145 wt % H_2O. Back-scattered electron image of 'K-rich spot', interpreted as quench from vapour phase in garnet lherzolite without melt or phlogopite. (h) P40, HZ2 +5% anhydrous phlogopite at 6 GPa, 1200°C, 0·145 wt % H_2O. Secondary electron image of 'Na- and K-rich spot', interpreted as quench from vapour phase (Vap) in garnet lherzolite without melt or phlogopite.

Table 1: Lherzolite compositions (wt %) prepared for this study

Starting composition	SiO_2	TiO_2	Al_2O_3	Cr_2O_3	FeO	MnO	MgO	CaO	Na_2O	K_2O	NiO	Total	Mg#
HZ1 (H&Z lherzolite)	46·20	0·18	4·08	0·40	7·59	0·10	37·96	3·23	0·33	0·03	0·28	100·2	89·9
HZ1 [analysed: see P77(1) in EA 4]	46·16	0·21	4·37	0·38	7·44	b.d.l.	37·33	3·31	0·53	b.d.l.	0·27	100·0	89·9
HZ2 (Fe-depleted H&Z lherzolite)	46·84	0·19	4·28	0·42	4·14	0·10	39·80	3·39	0·35	0·03	0·29	99·8	94·5
95% HZ1 + 5% 'anhydrous phlogopite'	46·01	0·17	4·50	0·38	7·18	0·10	37·46	3·05	0·31	0·62	0·27	100·1	90·3
MPY (Niida & Green, 1999)	44·74	0·17	4·37	0·45	7·55	0·11	38·57	3·38	0·40	0·00	0·26	100·0	90·1

H&Z, Hart & Zindler (1986); b.d.l., below detection limits; MPY, MORB Pyrolite.

from P77-1 but pargasite from O71 at 3 GPa, 1000°C (Supplementary Data EA 5) contains 1·1 wt % K_2O giving a modal abundance of 2·5–3 wt % pargasite [consistent with the modal and compositional variations of pargasite of Niida & Green (1999)]. After drying, and assuming that pargasite contains ~1·8 wt % H_2O, these starting materials contain ~0·27 and ~0·05 wt % H_2O in pargasite respectively and a further 0·02 wt % in NAMs (Kovács *et al.*, 2012) (i.e. 0·29 and 0·07 wt % H_2O respectively).

The bulk composition of our starting material was also checked by area scan (300 μm × 350 μm) analyses of P77-1. Agreement with the target HZ1 composition (Table 1) is within error for all oxides (P77-1; 'Area Scan' analyses in Supplementary Data EA 4) except that measured Na_2O contents are slightly higher than the target. This agreement underlies mass-balance calculations based on our mineral analyses and theoretical compositions (mix compositions) of Table 1. The confirmation of bulk composition in the study is important as the absence or paucity of Na_2O in clinopyroxene in experiments by Grove *et al.* (2006) using their anhydrous mix is a significant problem in reconciling the respective observations (Green *et al.*, 2012; Supplementary Data EA 2).

Experimental methods

Experiments were carried out in half-inch (1·27 cm) piston-cylinder apparatuses at the Research School of Earth Sciences (RSES), Australian National University (ANU). Standard 200 T presses were employed for 1·5–4 GPa runs, whereas a 500 T press (ultra-high-pressure press, labelled as UHPPC in Supplementary Data EA 3 and 4) and a shorter piston (2·2 cm instead of 3·8 cm) were used for 6 GPa runs. Experiments were run for 4·5 h to 7 days, with longer run times used for lower T and particularly for 'dry' experiments (Supplementary Data EA 3). Pressed salt (NaCl) external furnace sleeves with inner MgO-ceramic spacers, and graphite sleeves, were used as pressure media and heater, respectively. Temperature was controlled to ±10°C using a Eurotherm 904 controller and type B thermocouple ($Pt_{94}Rh_6$–$Pt_{70}Rh_{30}$). From temperature profiling of the furnace assembly, both thermocouple and sample lie within the 'hotspot' of the graphite heater so that sample and thermocouple temperatures are equated. The use of Au and Ag capsules prevented Fe loss in experiments at 1200°C or less (Hall *et al.*, 2004). Experiments above 1200°C at 4 GPa and all experiments at 6 GPa used AuPd double capsules rather than Au capsules to avoid melting of the capsule. As AuPd capsules may absorb Fe from the sample, the outer capsule contained a mix of fayalite + hydrous olivine basanite, which was either entirely liquid or contained crystals of olivine or olivine + magnetite in glass at the run conditions. Effectively this technique created an Fe gradient in the capsule so that empirically we observed that the Mg# of the HZ1 lherzolite in the inner capsule remained at Mg# = 90–93. Mineral analyses, specifically the stoichiometry of clinopyroxene and garnet, suggest the presence of small and significant Fe^{3+}. This may be due either to higher oxygen fugacity (f_{O2}) in AuPd capsules than in Au or Ag capsules, or to an increase of $Fe^{3+}/\sum Fe$ in mantle peridotite towards greater mantle depths as a consequence of relative volume changes (Gudmundsson & Wood, 1995; Frost & McCammon, 2008; Stagno *et al.*, 2013).

The use of 'melt-traps' and sample preparation techniques

As the detection, separation and analysis of near-solidus melts, or the detection of vapour and trapping of vapour-phase quench, was a key aspect of the study, several techniques for 'melt-traps' were evaluated by experiments on the HZ2 composition (Supplementary Data EA 5). Layers of carbon-glass spheres were trialled but showed precipitation in interstices of minerals that were distinctly lower in Cr than minerals in the lherzolite layer (Supplementary Data EA 5). Also, pargasite crystallized at 2·5 GPa, 1075°C (O72) whereas melt was present at 1050°C (O53) with olivine layers. The observations were consistent with transport of components (other than Cr) through a vapour phase of

lowered water activity. The carbon-glass spheres contain impurities, including metals, and are inferred to produce low f_{O2} conditions and a $(CH_4 + H_2O)$ vapour on the carbon saturation surface (see Taylor & Green, 1988) adding further complexity to the lherzolite + H_2O investigation. The experiments with carbon-glass spheres as a melt-trap were not used in mapping the phase relationships but are included in the data tables of Supplementary Data EA 3–5 as useful mineral parageneses.

An alternative approach is to use olivine, of composition similar to that in HZ1 lherzolite, as a melt or vapour trap inserted as a thin disc of 100–200 μm thickness (Odling *et al.*, 1997). This technique was adopted in two experiments on HZ2 composition with 2·9 and 7·25 wt % H_2O at 2·5 GPa, 1000°C (O60, O89), and an experiment with 2·9 wt % H_2O at 4 GPa, 1100°C (O61). Planes of very small fluid inclusions (breached) were observed on polished surfaces of the discs in all cases (Fig. 3). Doubly polished thin sections were prepared (O60, O89) and FTIR spectroscopy demonstrated spectra showing typical olivine absorption bands and also the broad band typical of molecular water—attributed to fluid inclusions visible in transmitted light along the IR transmission path (Kovács *et al.*, 2012). In subsequent experiments the olivine disc was replaced by layers of crushed San Carlos olivine (Mg# 90–91). We aimed at 1:2:1 to 1:1:1 proportions for mineral:lherzolite:mineral layers. These acted as a vapour- or melt-trap. The olivine layers were found to be analysable for water contents by FTIR spectroscopy (Kovács *et al.*, 2012). This technique was adopted for both melt-traps and FTIR analyses.

The success of the FTIR method led to a sample preparation routine for the layered capsules of mounting the unopened capsule in epoxy resin and polishing a longitudinal section. Polishing dry or under kerosene avoided possible solution of carbonate in water. This was followed by examination of this surface by scanning electron microscopy (SEM) imaging and micro-analysis of all phases. The specimen mount was then sliced to provide an ~70 μm thick doubly polished thin section, which was used for FTIR analyses of the melt-trap olivine layers and lherzolite layer. The remnant capsule, usually ~25% of the original capsule, was then repolished as 'reserve' material for further SEM work if required.

In experiments on HZ1 or HZ1 + phlogopite compositions the olivine in the lherzolite varies from Mg# 89·8 (P77-2, 1·5 GPa, 1000°C) to Mg# 90·9 (P77-1, 3 GPa, 950°C). The addition of olivine layers or discs with Mg# ~90 should make no detectable difference to phase compositions or proportions within the lherzolite layer for the HZ1 composition. This is confirmed by the data given in Supplementary Data Tables EA 4 and 5, including the matching of Ol-Lhz and Ol-L compositions in single experiments. For the higher Mg# HZ2 composition the reaction with layers of olivine Mg# ~90 composition alters the lherzolite phase compositions towards lower Mg# than observed in experiments without olivine layers (see Supplementary Data EA 5). Olivine contains only SiO_2, MgO, FeO and NiO above trace levels. The water content of San Carlos olivine is ~10 ppm and negligible in relation to added water. Ratios among the oxides H_2O, K_2O, Na_2O, CaO, Al_2O_3 and TiO_2 (which are important for issues of melting, vapour phase composition and clinopyroxene or pargasite composition) are unaffected by the addition or subtraction of olivine as long as all experiments have excess olivine in the lherzolite layer (which they do). Also, activities of MgO, FeO and SiO_2 are constrained by olivine + orthopyroxene saturation in all experiments. In contrast to olivine layers, the addition of orthopyroxene and clinopyroxene layers, including high- and low-Al examples, and with differing Na_2O and CaO contents (Kovács *et al.*, 2012, table 1) has observable effects on phase compositions, and even the presence or absence of pargasite or clinopyroxene in some experiments. It is emphasized that experiments with a pyroxene layer are not used to define phase relations, compositions or solidus temperatures of HZ1 or HZ2 (Kovács *et al.*, 2012, p. 2070). These experiments are used to measure water contents in pyroxene approaching equilibrium with phases in the mantle lherzolite composition at the same P–T. The mineral compositions were presented by Kovács *et al.* (2012, table 5) and are repeated in Supplementary Data EA 4 and EA 5 for ease of access to the mineral dataset.

The details of the FTIR techniques and results for measurement of water contents of minerals in the monomineralic layers have been presented by Kovács *et al.* (2012) and provide information on the storage of water in NAMs under conditions at which the roles of hydrous phases, water-rich vapour and water-rich silicate melt in model mantle lherzolite were monitored.

Analytical methods

The phase assemblages in our experiments were examined and analysed by SEM using a JEOL 6400 SEM with energy-dispersive X-ray spectroscopy (EDS) analysis or a Hitachi 4300 field emission SEM (FESEM). All facilities are housed in the Centre for Advanced Microscopy (CAM) of the ANU. Additional FESEM images used the Hitachi SU70 field emission SEM in the Central Science Laboratory at University of Tasmania. An accelerating voltage of 15 kV, beam current of 1 nA with a fully focused beam, and 120 s counting time were used for mineral analyses. Mineral analyses were screened for satisfactory stoichiometry before inclusion in the dataset. Analyses of interserts of quench phases derived from hydrous silicate or carbonate + silicate melts were done as area scans of appropriate size (usually <30 μm × 40 μm). Mineral standards produced by Astimex Scientific Limited were used to standardize mineral and glass analyses. Averages of

multiple analyses of each mineral phase and quenched liquid compositions are given in Supplementary Data EA 4 and 5. Detection limits are ~0·10 wt % for K_2O, TiO_2 and MnO, and ~0·15 wt % for Cr_2O_3 and Na_2O. The accuracy of the EDS and SEM methods used in this and similar studies from ANU has been demonstrated previously (Spandler *et al.*, 2010). In addition, in response to a reviewer comment that only wavelength-dispersive spectroscopy (WDS) analyses are of acceptable accuracy for publication (see also Till *et al.*, 2012*b*, p. 1084), our analytical methods using the JEOL 6400 SEM were applied to mineral standards (olivine, pyroxene, albite and garnet) circulated to and conventionally used in laboratories for WDS analyses all over the world. Results obtained are well within error for all oxides (Supplementary Data EA 6).

For several experiments with high water contents, the capsule was pierced under high vacuum at room temperature and the vapour released was semi-quantitatively analysed by gas chromatography. The vapour phase was dominantly water with minor carbon dioxide.

EXPERIMENTAL RESULTS

Textural observations, mineral phase stability and compositions

The full list of experiments of the study is given in Supplementary Data EA 3. All experimental products are well crystallized with grain sizes (10–30 μm) that are excellent for electron beam micro-analysis. Garnet and pargasite are commonly poikiloblastic with included olivine, orthopyroxene or clinopyroxene. Orthopyroxene and pargasite have a somewhat larger grain size than the other phases, but the textures of the experimental runs appear well equilibrated without large grain-size variation. SEM analyses confirm homogeneity of phase compositions. Experiments at 2·5 GPa, 1000°C in the 'dry' to 1·45 wt % H_2O range showed increasing porosity (voids or pits on polished surfaces) with increasing water contents. Experiments with >2·9 wt % H_2O were friable and capsules required piercing and vacuum impregnation with epoxy resin before opening the capsule. Otherwise the sample poured from the capsule as patchily agglutinated powder. Examination of the fracture surfaces of capsules with high water content showed euhedral crystals coated with fine fragments of glass 'froth'. Other euhedral crystals are draped with a thin glass film (Fig. 3). In experiments with high water contents, mineral segregation is noted with interlocking aggregates forming pyroxene-rich patches, and disaggregated olivine-rich patches [also noted by Grove *et al.* (2006)]. With five to seven phases in lherzolite in each experiment we sought to obtain up to five analyses of olivine and 5–10 analyses of other phases. Mineral analyses that did not have appropriate stoichiometry were eliminated before averaging. This was particularly necessary in identifying and eliminating poikiloblasic garnet areas with pyroxene inclusions. Mean compositions are listed in Supplementary Data EA 4 and 5. In experiments above the vapour-saturated solidus, in which quench aggregates of amphibole, clinopyroxene, oxide and carbonate are observed, the iron-rich (low Mg#) composition of the quench phase is readily distinguished from the equilibrated lherzolite phases. In these experiments the composition of the melt was estimated by area scan analyses (Mengel & Green, 1989) of quenched melt interserts trapped in olivine layers (Fig. 2; Supplementary Data EA 8).

Our principal use of the mineral composition data is in the variation of pargasite and clinopyroxene compositions with water content at temperatures below the silicate solidus. Mineral compositions are consistent throughout the lherzolite layer and good correlations exist between K_2O and Na_2O in pargasite and clinopyroxene and H_2O in the bulk composition (Fig. 4). The K_2O contents of olivine, orthopyroxene, clinopyroxene and garnet are below the limits of detection, as are the Na_2O contents of olivine, orthopyroxene and garnet in almost all analyses. Thus, it is possible to use these two oxides for estimation of modal pargasite and clinopyroxene abundances in subsolidus experiments at 3 GPa or less, in experiments with low water contents (<1·5 wt %). With higher water contents, the partitioning of K_2O and Na_2O into the vapour phase invalidates this simple mass-balance relation. Modal

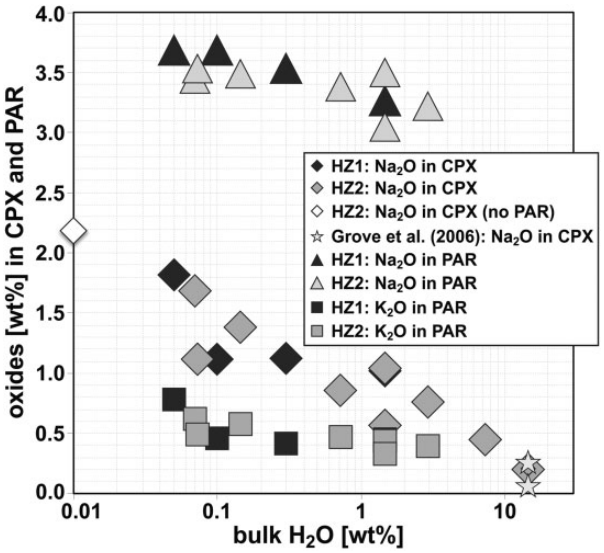

Fig. 4. Compositional variation in pargasite and clinopyroxene from subsolidus experiments at 2·4–2·5 GPa, 960–1100°C in HZ1 and HZ2 compositions, plotted against bulk water content (note logarithmic scale). The figure demonstrates the absence of pargasite at high water content correlating with diminishing Na_2O content in clinopyroxene. It should be noted that vapour is absent at <0·1 wt % H_2O approximately in HZ compositions.

abundances of the other phases were calculated by least-squares mass-balance calculations using StatPlus for Mac (similar to Microsoft Excel®) incorporating average phase compositions, and appropriate bulk composition (i.e. HZ1, HZ2 or HZ1 +5 wt % anhydrous phlogopite).

In presenting our experimental results, we have placed the discussion of the experiments duplicating the methods of Grove *et al.* (2006) in Supplementary Data EA 2. Summarizing this material: using the mix HZ2 +14·5 wt % H_2O, our observations closely reproduce those of Grove *et al.* (2006), particularly the absence of pargasite at pressures >2 GPa and the very low Na_2O content of clinopyroxene. We also observe siliceous glass 'froth' within voids among intergrown olivine, ortho- and clinopyroxene and garnet, and as thin films coating euhedral minerals. However, using the 'dry' mix at 2·4 GPa, 1100°C (O16), clinopyroxene contains 2·19 wt % Na_2O in our experiment, whereas at the same P–T conditions Grove *et al.* (2006) reported 0·07 wt % Na_2O, which does not give satisfactory mass balance. The problem of 'missing' Na_2O in all experiments by Grove *et al.* (2006) using the dry mix is unresolved (see also Green *et al.*, 2012).

Our remaining data are discussed below, beginning with experiments at 2·5 GPa in which we varied water content from 'dry' to 14·5 wt % H_2O.

Experimental results at 2·5 GPa

Pargasite stability with or without an aqueous vapour phase

At 2·5 GPa, 1000°C pargasite is absent from experiments on HZ2 composition with 14·5 and 7·25 wt % H_2O but is present in all experiments on both HZ1 and HZ2 compositions with 2·9 wt % or lower H_2O contents, including a nominally 'dry' experiment. The K_2O content of pargasite increases as the water content of the bulk composition decreases, to 0·62 wt % in the 'dry' experiment (O65) at 1000°C (Supplementary Data EA 5) and 0·78 wt % in the experiment (P78) with 0·05 wt % H_2O at 1050°C (Fig. 4; Supplementary Data EA 4). There is only 0·03 wt % K_2O in the HZ1 and HZ2 lherzolite compositions and by simple mass balance of K_2O we infer ~5 and ~4 wt % modal pargasite respectively in these experiments. It should be noted that if clinopyroxene contained 0·05 wt % K_2O (i.e. below the detection limit) the estimates of modal pargasite would decrease to ~4 and ~3·5% respectively. In the experiment with 0·073 wt % H_2O (O57) the pargasite contains 0·5 wt % K_2O and we infer ~6 wt % modal pargasite. From stoichiometry and from analyses of natural pargasites, we infer that pargasite contains 1·5–2·0 wt % H_2O and, with 6% modal pargasite, accounts for ~0·1 wt % H_2O in the bulk composition. NAMs may contain additional H_2O (~0·02 wt %; Green *et al.*, 2010, 2011; Kovács *et al.*, 2012). Therefore experiments with less than ~0·12 wt % H_2O are vapour-undersaturated and those with more than ~0·12 wt % H_2O in the sample must have additional water in a fluid (melt or vapour) phase. There is no evidence for a hydrous silicate melt using the criteria noted above and our observations from the olivine disc and melt-trap experiments (see next section) are clearly indicative of an aqueous vapour phase (Fig. 3) at 1000°C in the experiments with >0·12 wt % H_2O.

In experiments with 0·145, 0·3, 0·725, 1·45 and 2·9 wt % H_2O, K_2O is partitioned between pargasite and an increasingly water-rich vapour phase (Fig. 5). In addition, the Na_2O contents of both pargasite and clinopyroxene, and the Al_2O_3 content of clinopyroxene, decrease with increasing H_2O content of the sample (Fig. 4; Supplementary Data EA 4 and 5). These observations are consistent with an increase in the modal abundance of the vapour phase and a dilution of Na_2O and K_2O in the vapour phase; that is, inferring constant partition between vapour and clinopyroxene or pargasite. The systematic behaviour of K_2O and Na_2O with increasing water content includes both HZ1 and HZ2 compositions, confirming that the small differences in Mg# and olivine/orthopyroxene ratio do not significantly affect phase relationships. We infer that as K_2O and Na_2O are partitioned between pargasite, clinopyroxene and vapour phase, increasing H_2O in the bulk composition results in leaching of these oxides into the vapour phase, decreasing their concentration in pargasite (K_2O, Na_2O) and clinopyroxene (Na_2O). Extraction of Na_2O and K_2O into the aqueous vapour phase and dilution by increasing water content results in the destabilization of pargasite between bulk water contents of 2·9 and 7·25 wt % H_2O. Whereas clinopyroxene remains stable with increasing water content, the jadeite solid solution ($NaAlSi_2O_6$) decreases and at the highest water content (14·5 wt % H_2O) clinopyroxene has an Na_2O content approaching our detection limit. The dependence of pargasite stability or instability on H_2O content is also illustrated by two experiments (O24, O17) at 2·4 GPa, 960°C with 1·45 wt % H_2O (pargasite present) and 14·5 wt % H_2O (pargasite absent), respectively [reproducing the Grove *et al.* (2006) experiment C245; Supplementary Data EA 5]. By varying the water content, we have demonstrated that pargasite is stable with excess vapour up to ~5 wt % H_2O, but at higher water contents, pargasite is absent, clinopyroxene approaches Na-free diopside (Supplementary Data EA 5) and a coexisting aqueous vapour contains dissolved components, particularly Na_2O, K_2O, SiO_2, and Al_2O_3.

The stability, composition and modal abundance of pargasite are closely matched to observations on lherzolite (MOR Pyrolite) by Niida & Green (1999) for 'water-saturated' and 'water-undersaturated' conditions, and by Fumagalli *et al.* (2009) also on a MOR Pyrolite composition. Attention is drawn to our new experiments with 'dry' composition at 2·5 GPa, 1100°C (O16) and with

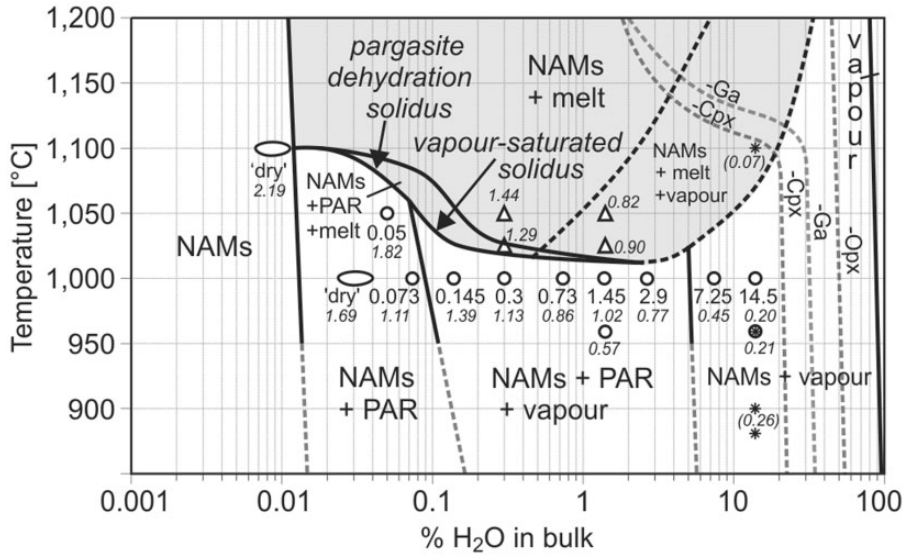

Fig. 5. Diagram at ~2·5 GPa illustrating phase stability as a function of water content (note logarithmic scale) and temperature, based on the experimental results on HZ1 and HZ2 compositions and prior studies, particularly those by Niida & Green (1999) and Grove *et al.* (2006). Triangles, experiments in which a water-rich silicate melt was observed in HZ1 composition; circles, experiments in HZ1 or HZ2 compositions with a water-rich vapour (porous and with fluid inclusions or vapour phase quench); ellipses, 'dry' experiments (no added water). Numbers below data points at 1000°C are added water contents of experimental runs and numbers in italics are Na_2O contents of clinopyroxenes (Fig. 4; Supplementary Data EA 4 and 5). Asterisk symbols and associated Na_2O contents (in parentheses) are from Grove *et al.* (2006).

0·05 wt % H_2O at 1050°C (P78). These conditions are below the dehydration-melting solidus (or 'water-undersaturated' solidus) of Niida & Green (1999). Melt is not observed in either experiment. Pargasite is absent at 1100°C, 'dry' (O16), and only ~4 modal % pargasite with 0·78 wt % K_2O is present in P78. Both these experiments and two experiments at 1000°C 'dry' and with 0·073 wt % H_2O (O65, O57), may be described as vapour-absent in that all water is structurally bound in pargasite and NAMs.

The appearance of pargasite and of water in NAMs (see Kovács *et al.*, 2012) in nominally 'dry' experiments requires comment. The modal abundance of pargasite is ~4–5% and assuming a water content in pargasite of 1·5 wt % H_2O, the bulk water in the 'dry' experiment is ~0·07%. The water content of San Carlos olivine is ~10 ppm (Kovács *et al.*, 2008) and is relatively insignificant. The source of water in 'dry' experiments may be from hydrogen migration through the capsule walls in long duration experiments. The magnitude of this 'background water' is of the same order as the minimum 'added water' (0·05 and 0·073 wt % H_2O) and essentially defines a limit to achieving 'dry' conditions at long run times by our experimental techniques [i.e. also as reported by Rosenthal *et al.* (2014)].

'Water-saturated solidus'—hydrous silicate melt or aqueous vapour with dissolved oxides?

We conducted experiments at 2·5 GPa with three water contents (1·45, 0·3 and 0·05 wt % H_2O) to locate the solidus. With 1·45 wt % H_2O, pargasite is present at 1000°C in both HZ1 and HZ2 compositions (Supplementary Data EA 4 and 5; Figs 4 and 5) and there are no quench interserts of iron-enriched amphibole, carbonate and glass (i.e. no quenched hydrous silicate melt). As the modal proportion of pargasite is ~7% (Supplementary Data EA 4 and 5) we can estimate the water locked in pargasite as ~0·11 wt %, with a further 0·02% approximately in NAMs at this P and T (Kovács *et al.*, 2012). Thus the experiments with 1·45 wt % added water are clearly vapour-saturated with >1·3 wt % of a separate vapour phase in the experiments. Also, experiments on HZ1 with 0·3 wt % water are vapour-saturated but with only ~0·2 wt % vapour. At 1025 and 1050°C, experiments show the penetration into the olivine layers by hydrous silicate melt, quenching to more Fe-rich amphibole + oxide + dolomite aggregates. This is demonstrated in the experiments above 1000°C with olivine layers (O52, O53, P79, P81, O79, O77). The solidi of both HZ1 and HZ2 lherzolites in the presence of water-rich vapour (1·45 wt % H_2O in bulk composition) are between 1000 and 1025°C. At 1025°C, 1·45 wt % H_2O, pargasite is present with melt in the more magnesian composition HZ2 but absent from HZ1 composition. Pargasite is absent from both compositions at 1050°C. Three experiments, P80, P81 and P79, were carried out on HZ1 composition with 0·3 wt % H_2O, at 1000, 1025, and 1050°C. The vapour-saturated solidus is again inferred to be between 1000 and 1025°C with a small field of coexisting pargasite + melt

(vapour-undersaturated) immediately above the solidus (Supplementary Data EA 4; Fig. 5).

In the experiment (P78, HZ1, EA 4) at 1050°C with 0·05 wt % H_2O, pargasite is present, whereas hydrous silicate melt and water-rich vapour are absent. The experiment is below the dehydration-melting solidus. Consistent with this, pargasite has the highest K_2O (0·78 wt %) and lowest modal abundance (4%) of all 2·5 GPa experiments. Also, the coexisting clinopyroxene has 1·82 wt % Na_2O, a value exceeded only by the clinopyroxene (2·19 wt % Na_2O) in the pargasite-free, 'dry' experiment at 2·4 GPa, 1100°C (O16).

The detailed examination of run products shows that the solidus of pargasite lherzolite at 2·5 GPa is not independent of the amount of water present (Fig. 5) but decreases in temperature towards the vapour-saturated solidus as water content increases from 'dry' through water-deficient (dehydration solidus) to excess water (the 'vapour-saturated' solidus). From ~0·145 to 1·45 wt % H_2O in HZ1 and HZ2 lherzolites the solidus is vapour-saturated and lies between 1000 and 1025°C.

Effects of carbonate contamination

The presence of a very small carbon (carbonate) content in our experiments introduces detectable quenched carbonatite melt at conditions below the appearance of hydrous silicate melt, particularly in experiments with very low water contents. The carbon(ate) may have been introduced by MgO or $Mg(OH)_2$, or retained in alkali carbonates used to prepare the starting compositions, or may be a consequence of starting compositions being mixed under acetone and dried under reducing conditions. Using the fertile Hawaiian Pyrolite composition (Green & Wallace, 1988; Wallace & Green, 1988; Falloon & Green, 1989, 1990) and other compositions (Thibault *et al.*, 1992; Yaxley & Green, 1996) it has previously been shown that the Lherzolite + H_2O + CO_2 solidus at 2·5 GPa is at ~930°C, which is below the Lherzolite + H_2O solidus at 1000–1025°C. The melt at the solidus is a sodic, dolomitic carbonatite. An important observation in these studies is that subsolidus dolomite or magnesite is always more magnesian than coexisting olivine or pyroxenes whereas the converse applies for carbonate from quenched carbonatite melts. Using high-magnification SEM, we find uncommon interstitial quench dolomite (i.e. with Mg# <88) with minor oxide, and with Na enrichment on neighbouring crystal terminations, in experiments at 1000°C. The quench carbonate is particularly evident at very low H_2O contents and in the presence of pargasite; that is, with higher CO_2/H_2O (see also Wallace & Green, 1988). The fraction of carbonatite quench is much less (≪1 wt %) than the quenched melt (quench amphibole + oxide + minor dolomite + outgrowths on neighbouring silicate crystals) in intersertal texture, which is present in experiments at temperatures above the pargasite breakdown (Fig·2).

The observations on the series of experiments at 1000°C demonstrate the absence of a hydrous silicate melt at this temperature for any water content (Fig. 5). However, we identify an unintended very small carbonatite melt with pargasite at <0·3 wt % H_2O.

Compositions of melts near the vapour-saturated solidus

In the experiments on HZ1 with different water contents at 1050°C, pargasite is present and quenched melt is absent with ~0·05 wt % H_2O (P78). Mass-balance estimations based on Na_2O and K_2O contents are 4% pargasite and 10% clinopyroxene. Quench from hydrous silicate melt is present in the other experiments at 1050°C with higher water contents, and we have used area scan analyses, Mg# vs oxide plots (Supplementary Data EA 7) and K_d (Ol/Liq) relationships to estimate liquid compositions for 0·3 wt % H_2O (P79) and 1·45 wt % H_2O (O77) in HZ1 composition and for 1·45 wt % H_2O (O53) in HZ2 composition. These estimated melt compositions are listed in Supplementary Data EA 4 and 5. It should be noted that the melt composition in P79 is transitional between carbonatite and olivine melilitite whereas the melts in O77 and O53 are basanite to olivine nephelinite, based on normative components. From these melt compositions and the analysed clinopyroxene compositions, the melt fractions are estimated (using mass balance with Na_2O and K_2O contents) as ~1·7% melt for 0·3 wt % H_2O (P79) and 2·2% melt for 1·45 wt % H_2O (O77), with ~10% clinopyroxene in the residual lherzolite. Both these melt compositions are at 1050°C.

In an experiment on HZ1 at 1025°C, with 1·45 wt % H_2O (O79), pargasite is absent, clinopyroxene has 0·9 wt % Na_2O and the experiment is clearly above the hydrous silicate melt solidus (see the SEM images in Supplementary Data EA 8). However, in HZ1 composition at the same P and T, with 0·3 wt % H_2O (P81), hydrous silicate melt is present with pargasite and clinopyroxene. Estimates of 2·5% pargasite, 10% clinopyroxene and 1% melt are consistent with phase compositions and phase assemblages of neighbouring experiments.

The two sequences of experiments through the hydrous silicate melt solidus (HZ1) with 0·3 and 1·45 wt % H_2O respectively show significant differences in melt fraction and composition, and in clinopyroxene compositions (Supplementary Data EA 4). With 0·3 wt % H_2O in the charge, if the melt fraction increases from 1·5 to 2% with ~25 wt % H_2O in the melt, the melt becomes 'water-undersaturated'. However, with 1·45 wt % H_2O in the charge (O85, O79, O77), pargasite is present at 1000°C (O85) but absent at 1025°C (O79) and 1050°C (O77). If the near-solidus basanitic melt contains ~25 wt % H_2O (Green, 1973*a*; Nicholls & Ringwood, 1973; Green *et al.*, 1975, 2001; Edgar *et al.*, 1976; Brey & Green, 1977; Irving &

Green, 2008) then the estimated 2·2% melt does not contain all the water in the charge and ~6% melting is required before an aqueous vapour phase is eliminated. By contrast, the solidus of HZ1 with only 0·3 wt % H_2O is also between 1000 and 1025°C and is vapour-saturated ($H_2O + CO_2$) but becomes vapour-undersaturated immediately above the solidus (Fig. 5).

In presenting our estimates of near-solidus melt compositions we have used conventional normative expressions of the chemical compositions and corresponding petrological terms: for example, 'basanitic' indicating similar proportions of normative nepheline and albite; 'nephelinitic' indicating dominant nepheline with minor albite or larnite; 'melilitic' for significant normative larnite. However, it is not suggested that these near-solidus melts equate to observed mantle-derived olivine-rich basanites, olivine nephelinites and olivine melilitites as commonly observed as intraplate, mantle-xenolith-bearing magmas. The vapour-saturated near-solidus melts from ~2·5 GPa, or less, will begin to crystallize and de-gas on separation and ascent, even if their cooling path is adiabatic. The melts near the vapour-saturated solidus that we observe in our experiments are significant for the roles that they may play in mantle metasomatism, and in wall-rock reaction with ascending mantle diapirs or magma channels.

Phase relationships of HZ1 and HZ2 lherzolites at 2·5 GPa at high water contents

The experimental data demonstrate the role of the excess aqueous vapour (with minor CO_2) at 1000°C in leaching K_2O and Na_2O from their subsolidus host phases, pargasite and clinopyroxene. At 2·4 GPa, 960°C and 2·5 GPa, 1000°C, experiments with high (7·25 and 14·5 wt %) H_2O contents (O17, O89, O50; Supplementary Data EA 4 and 5) do not contain pargasite. With 14·5 wt % H_2O (O50), clinopyroxene has ~0·2 wt % Na_2O and samples contain common glass films and 'froth' coating euhedral minerals, with abundant void space. In the study by Grove *et al.* (2006) at 2·4 GPa with 14·5 wt % H_2O, experiments at 1100, 900 and 880°C do not contain pargasite and have >10% clinopyroxene with 0·07 wt % Na_2O (1100°C) and 0·26 wt % Na_2O (900°C). As there are no phases other than clinopyroxene and the aqueous phase that contain Na_2O, we can use the estimated modal abundance (~10–13%) of clinopyroxene from both studies to calculate an approximate molar H_2O/Na_2O of the aqueous phase as ~100 in the experiment with 7·25 wt % H_2O and as ~160 in the experiment with 14·5 wt % H_2O. These values are indicative of aqueous vapour (fluid) rather than water-saturated silicate melt, as studies of olivine-rich basalt + H_2O at similar pressures show that vapour-saturated melts have molar H_2O/Na_2O ~15–20 (Green, 1973*a*; Brey & Green, 1975, 1977; Irving & Green, 2008).

The experiments with 14·5 wt % H_2O by Grove *et al.* (2006) also constrain the disappearance of clinopyroxene by melting reactions to be above 1100°C. At this T and water content, the clinopyroxene is approaching diopside composition with negligible sodium, and the melting behaviour approaches that of $CaO–MgO–Al_2O_3–SiO_2–H_2O$ (Adam, 1988). No data were provided on the compositions of fluid and/or the melt inferred to be present from 880 to 1060°C (Till *et al.*, 2012*a*). Differences in glass morphology in the study by Till *et al.* (2012*a*) were interpreted by those researchers as evidence for two fluid phases (hydrous silicate melt and aqueous vapour) in the experiments at 1060 and 1100°C, 3·2 GPa, but similar textures were not presented for lower temperatures. Both garnet and clinopyroxene disappear between 1100 and 1125°C and the modal abundance of melt at 1125–1175°C is estimated as 23–25%. The published results of Grove *et al.* (2006) and Till *et al.* (2012*a*) for experiments at 2·4 and 3·2 GPa with 14·5 wt % H_2O can be reinterpreted as subsolidus with an aqueous vapour phase present up to ~1050°C, and with vapour-saturated hydrous silicate melt at >1050°C. Because of the solution of Na, K and other components into the aqueous vapour phase, the condensed phases approach the $CaO–MgO–Al_2O_3–SiO_2–H_2O$ system in which water-saturated melting begins at ~1050°C (Adam, 1988).

The phase relations in the presence of various amounts of water in the system lherzolite + H_2O are illustrated in Fig. 5. At water contents >5 wt % H_2O pargasite is absent and the solidus is that of a four-phase lherzolite in which clinopyroxene has decreasing jadeite solid solution (Na_2O and Al_2O_3 contents) and the vapour phase has increasing H_2O/Na_2O. Thus, the inferred solidus for high water contents in the revised figure (see Green *et al.*, 2010) is drawn with gradually increasing T from a minimum for the pargasite lherzolite + vapour assemblage to a value approaching 1100°C estimated for the Na_2O-free $CaO–MgO–Al_2O_3–SiO_2–H_2O$ (CMASH; Adam, 1988). In the CMASH system with excess water, garnet and diopside are expected to disappear very close to the solidus if melts are broadly basaltic (i.e. have high Ca and Al contents) relative to lherzolite composition.

The boundary between vapour-saturated and vapour-undersaturated melt fields was intersected in near-solidus runs with 0·3 and 1·45 wt % H_2O as discussed above. The approximate position of the boundary between these fields at higher temperatures is inferred from earlier studies at 2–3 GPa in which the maximum water contents (and consequent liquidus depression) for olivine-rich melts were demonstrated to be 25–30 wt % H_2O (Fig. 1). Thus for a given bulk water content in Fig. 5 the saturation boundary for appearance of a separate vapour (fluid) in addition to water-rich silicate melt is drawn at ~25 wt % H_2O dissolved in the melt phase, any larger water content appearing as a separate vapour (fluid) phase.

Experimental results at 1·5 GPa

The purpose of an experiment (P77-2) at 1·5 GPa, 950°C, with ~1 wt % H_2O was to synthesize pargasite lherzolite containing ~15–20 modal % pargasite following the results of Niida & Green (1999). A well-crystallized assemblage of olivine + orthopyroxene + clinopyroxene + pargasite + spinel was obtained in which pargasite contained 2·45 wt % Na_2O and 0·2 wt % K_2O. Using these oxides to calculate modal proportions yields an estimate of 14·7% pargasite and 6·5% clinopyroxene (Supplementary Data EA 4). Assuming ~1·5–2 wt % H_2O in pargasite and ~0·02 wt % H_2O in NAMs, the water content of the synthesized pargasite lherzolite after drying at 200°C is ~0·3 wt % H_2O. This material, together with pargasite lherzolite (P77-1) containing ~0·05 wt % H_2O synthesized at 3 GPa, 950°C, was used to evaluate the dehydration solidus of pargasite lherzolite at 1·5 and 2·5 GPa. When rerun at 1·5 GPa, 1025°C (P82, P83), both starting materials yielded pargasite-bearing spinel lherzolite. Olivine melt-trap layers were used in both experiments. Experiment P82 contains ~7 modal % pargasite (containing 0·4 wt % K_2O) with no evidence for quenched silicate melt in the melt-trap layer.

In the more water-rich composition (P83) at 1025°C pargasite has no detectable K_2O and quenched silicate melt in intersertal texture is present in the olivine layers; that is, it is above the solidus. The P–T conditions of the experiment are at pressures below the carbonation–decarbonation reactions (olivine + clinopyroxene + CO_2 = orthopyroxene + dolomite) in lherzolite (Wyllie *et al.*, 1983; Falloon & Green, 1989, 1990) and thus, noting the presence of small CO_2 contents in our experiments, as discussed previously, we expect the presence of a small amount of CO_2-rich vapour in subsolidus experiments at 1·5 GPa. We interpret P83 as above the solidus for a (CO_2 + H_2O) vapour, and interpret P82 (with ~0·05 wt % H_2O) as below the solidus for a more CO_2-rich vapour. It should be noted that our results, including the compositions of pargasite and clinopyroxene, and the presence of a very small melting interval in which melt and pargasite coexist, closely match those of Niida & Green (1999) on the slightly more sodic MOR Pyrolite composition (0·4 rather than 0·33 wt % Na_2O; Table 1). At 1·5 GPa, because pressures are below the carbonation reactions for lherzolite, the effect of CO_2 vapour is to raise the solidus for hydrous silicate melt, carbonatite melt being unstable in lherzolite at this pressure (Wallace & Green, 1988; Falloon & Green, 1989, 1990; Tumiati *et al.*, 2013).

As it was possible to analyse spinel coexisting with olivine and orthopyroxene at 1·5 GPa in both P82 and P83, we calculate f_{O2} in each case from the estimated magnetite solid solution (Ballhaus *et al.*, 1990). The calculated f_{O2} values are 0·6 log units below the fayalite + magnetite + quartz buffer or 3·5 log units above the iron + wüstite buffer (i.e. $\log f_{O2} = -10{\cdot}3$).

Experimental results at 3 GPa

An experiment with HZ2 composition at 3 GPa, 1000°C containing 0·145 wt % H_2O (O71) yielded olivine + orthopyroxene + clinopyroxene + garnet + pargasite. Pargasite is distributed throughout the charge and is homogeneous in composition. Pargasite contains 1·1 wt % K_2O and 3·64 wt % Na_2O. Clinopyroxene has 1·91 wt % Na_2O, slightly less than in clinopyroxene analysed in the dry garnet lherzolite (O16, HZ2 at 2·4 GPa, 1100°C; estimated mode has 16% clinopyroxene). Using mass balance for K_2O and Na_2O, the modal abundances of pargasite and clinopyroxene are ~2·7% and ~13% respectively. Assuming that pargasite contains 1·5 wt % H_2O, then ~0·04 wt % H_2O is in pargasite, ~0·02 wt % H_2O is in olivine + orthopyroxene + clinopyroxene + garnet (NAMs: see Green *et al.*, 2010, 2011; Kovács *et al.*, 2012) and ~0·085 wt % H_2O is present in excess (i.e. as a vapour phase).

Experimental results at 4 GPa

Till *et al.* (2012*a*) placed the water-saturated solidus between 800 and 820°C at 4 GPa based on experiments with 14·5 wt % H_2O. We have carried out experiments at higher temperatures but lower water contents, which, if the Grove *et al.* (2006) and Till *et al.* (2012*a*) interpretations are correct, should contain hydrous silicate melts. Alternatively, such experiments should reveal evidence for an aqueous vapour phase. Our first experiment (O61) at 4 GPa, 1100°C was with the HZ2 + 2·9 wt % H_2O composition, and with an olivine disc inserted in the charge. The garnet lherzolite assemblage contains clinopyroxene with 0·7 wt % Na_2O. With 0·33 wt % Na_2O in the bulk composition and no other crystalline phase containing Na_2O, mass balance would require ~50% clinopyroxene. This is not the case and at least half the sodium is present in a vapour–fluid or melt phase. Potassium was below the limit of detection in all crystalline phases and was presumably partitioned into a vapour or melt phase. Polished thin sections showed trains of very small fluid inclusions within or exposed at the surface of the olivine disc. These fluid inclusions were very clearly seen in transmitted light in the doubly polished thin sections for FTIR studies (Kovács *et al.*, 2012). There were no inclusions that showed quench intergrowths of silicates, carbonate and oxide, either in the olivine disc or in intersertal texture in the lherzolite layer.

Two further experiments were conducted at 4 GPa, 1100°C with HZ1 composition and 1·45 wt % H_2O (O80) and 0·145 wt % H_2O (O92). These experiments contained top and bottom layers of crushed olivine as 'melt-traps'. Both crystallized as garnet lherzolite with clinopyroxene containing 1·02 and 1·77 wt % Na_2O respectively.

Potassium was below the limit of detection in all analyzed phases of both experiments. No silicate, carbonate and oxide quench aggregates were observed in grain interstices of the olivine melt-traps. We infer that the experiments are subsolidus (i.e. there is no silicate melt present) and the water added to the charge is present as a vapour phase in which there are dissolved oxides, particularly Na_2O and K_2O. Mass balance for Na_2O alone is satisfied for O92 (0·145 wt % H_2O) if there is 19 modal % clinopyroxene, but inclusion of other oxide and silicate phases in mass-balance calculations shows that clinopyroxene cannot be greater than ~15 modal %,; that is, a small amount of sodium is present in an additional phase. With even lower Na_2O contents in clinopyroxene of O80 and O61, mass balance in these more water-rich experiments (1·45 wt % and 2·9 wt % H_2O respectively) cannot be satisfied without an additional Na-bearing phase. The correlation between decreasing sodium content of clinopyroxene and increasing bulk water content parallels the observations at 2·5 GPa (Fig. 4) and argues for the presence of a water-rich vapour in which sodium activity decreases with increasing bulk water content. Two experiments were carried out at 4 GPa, 1150°C with 1·45 wt % H_2O using HZ1 (O78) and HZ2 (O76) composition, and with olivine melt-trap layers in each. No interserts with quench amphiboles were observed in the olivine layers, but polished mounts showed very small fluid inclusions exposed in some olivine grains. The garnet lherzolite assemblage was observed in each experiment with clinopyroxene with 1.0 wt % Na_2O in O78 and 1·9 wt % Na_2O in O76.

The experiments with 1·45 wt % H_2O at 4 GPa, 1200°C (O81, Au capsule) and 1225°C (O98, AuPd capsule) used olivine layers as melt-traps and indicators of water in NAMs. However, a modification of methods was required following a failed experiment using a gold capsule at 1250°C in which the capsule melted. Thus at 1225°C, the double capsule technique using Au–Pd capsules with an Fe-enriched hydrous basanite in an outer capsule as a barrier to Fe-loss was effective in maintaining the Mg# of olivine and pyroxenes at ~90·9. The experiment at 1200°C is very similar to those at 1100 and 1150°C, with mineral analyses also being similar except for increasing CaO in orthopyroxene and decreasing CaO in clinopyroxene as T increases. Clinopyroxene has similar Na_2O content to that in experiments with 1·45 wt % H_2O at lower temperatures. There are no interserts of quench silicates in the olivine layers and the olivine and lherzolite layers are porous with evidence for local 'high' values of K or Na at clinopyroxene crystal faces in pores (i.e. indicative of quench from a vapour phase).

At 1225°C (O98) there are distinctive interserts with quench amphibole between olivine grains in both upper and lower olivine layers. The quench amphibole is enriched in Na, K, Ca, and Ti and, importantly, has Mg# ~63 (Supplementary Data EA 4), considerably below values for the lherzolite minerals, including garnet. We observed qualitatively that there was Fe-enrichment on some grain boundaries and analysable quench pyroxene as clinopyroxene outgrowths. In comparison with lower T experiments, clino- and orthopyroxene show decreased and increased CaO content respectively. We infer that a hydrous silicate melt is present at 1225°C and is in equilibrium with a garnet lherzolite residue in which clinopyroxene contains 1·2 wt % Na_2O. If the near-solidus melt contains ~30 wt % H_2O then HZ1 lherzolite would have a maximum of ~5 modal % melt (i.e. no excess vapour phase) in experiment O98 with 1·45 wt % H_2O at 4 GPa, 1225°C. The calculated melt composition from area scan analyses (Supplementary Data EA 4) has ~0·77% K_2O, indicating ~4 modal % melt.

Accordingly we locate the vapour-saturated solidus at 4 GPa between 1200 and 1225°C. We emphasize the textural distinction between experiments at and below 1200°C, in which there are no interserts of 'silicate (Fe-enriched amphibole or clinopyroxene) + carbonate + oxide' (i.e. quenched hydrous silicate melt) in the olivine melt-trap layer, and that at 1225°C, in which such texture is well developed.

As Till *et al.* (2012*a*) presented a sequence of experiments from 760 to 1100°C at 4 GPa on HZ1 +14·5 wt % H_2O, it is possible to directly compare their results with our data obtained with 0·145, 1·45 and 2·9 wt % H_2O. Till *et al.* (2012*a*) interpreted two experiments at 760 and 800°C as subsolidus and that at 820°C as above solidus. All three experiments through the inferred solidus contain clinopyroxene with very low Na_2O contents (0·29, 0·16 and 0·1 wt % Na_2O) and modal or mass-balance calculations show that, whether interpreted as subsolidus or 'above solidus', most of the Na_2O must be in the vapour–fluid or 'melt' phase. A similar conclusion follows from their experiments at 3·6 GPa, 800°C (subsolidus) and 840°C (interpreted as above solidus) in which clinopyroxenes are equally low in Na_2O (0·23 and 0·28 wt % Na_2O respectively). No mineral analyses were reported for experiments between 820 and 1100°C, and at 1100°C clinopyroxene is absent and a quench Ca-rich carbonate (Mg# ~65) is present. Although the 1100°C experiment was interpreted as 'melt present' no analytical data or high-magnification SEM images were provided. Our preferred interpretation of this experiment is that it contains a single fluid (vapour) phase with dissolved oxides including SiO_2, Na_2O, CaO, and Al_2O_3. Comparing the four experiments from the two studies at the same conditions (4 GPa, 1100°C) and with 0·145, 1·45, 2·9 wt % (this study) and 14·5 wt % H_2O (Till *et al.*, 2012*a*), the Na_2O contents of clinopyroxene decrease (1·8%, 1·0%, 0·7% and zero respectively) and clinopyroxene is destabilized as water content increases. We interpret these observations as a subsolidus leaching effect

of increasing water/rock ratio and high solubility of oxide components in aqueous vapour at high P and T. In lower T experiments at 4 GPa, the vapour phase solubility of Na_2O in particular remains sufficiently high to 800°C so that with 14·5 wt % H_2O in experiments, clinopyroxene contained <0·3 wt % Na_2O (Till *et al.*, 2012*a*).

Experimental results at 6 GPa

The experiments at 6 GPa were aimed at detection of the first appearance of hydrous silicate melt with increasing temperature above 1300°C, and the simultaneous determination of water contents in olivine layers or alternatively in olivine and low-alumina orthopyroxene layers. Experiments with olivine layers at 1300, 1350 and 1400°C with either 1·45 or 0·145 wt % H_2O obtained well-crystallized garnet lherzolite. The recrystallized olivine layers contained very small interstitial aggregates of quench dolomite and Fe-rich oxide at 1300°C (P53) and 1350°C (P51), interpreted as quenched carbonatitic melt. However, at 1400°C (P49, Fig. 1) much larger intersertal patches of finely intergrown quench amphibole or clinopyroxene, carbonate and Fe–Ti oxide were observed and interpreted as quenched hydrous silicate melt, also originally containing dissolved carbonate. Two further experiments at 1350°C (P21) and at 1400°C (P47), both with 1·45 wt % H_2O, used olivine and low-alumina orthopyroxene layers to allow measurement of water partitioning between olivine and orthopyroxene (Kovács *et al.*, 2012). At 1350°C (P21), the lherzolite layer crystallized as garnet lherzolite and both orthopyroxene and olivine layers contained very small intergranular areas of quench carbonate (i.e. similar to P51). Minor garnet appeared in the orthopyroxene layer and is more Cr-rich than that in the lherzolite layer.

At 1400°C, the lherzolite layer between olivine layers (P49) crystallized as garnet lherzolite with subcalcic diopside. However, in P47 with olivine + orthopyroxene layers, clinopyroxene is absent from the original lherzolite layer. The recrystallized orthopyroxene in the orthopyroxene layer has increased its CaO content relative to the starting composition, and is inferred to have effectively dissolved the clinopyroxene from the lherzolite layer in adjusting to the overall bulk composition. Both experiments have large interserts of intergrown silicate, oxide and carbonate, which are inferred to be quench products from interstitial carbonate-bearing hydrous silicate melt. The transition from a trace of carbonatite melt (probably with excess water-rich vapour) to hydrous silicate melt with dissolved carbonate is inferred to be between 1350 and 1400°C at 6 GPa.

In an attempt to eliminate carbonate, three experiments were carried out by adding ~1 wt % H_2O by micropipette to the anhydrous mix rather than by adding the mix containing $Mg(OH)_2$. Experiments at 1350°C (P84), 1400°C (P86) and 1450°C (P85) had one layer of olivine only and were unsuccessful in eliminating trace carbon (carbonate). All contain garnet lherzolite assemblages in which the clinopyroxenes are subcalcic and coexisting orthopyroxenes have relatively high CaO contents. Clinopyroxenes in these experiments and in those with 1·45 wt % H_2O contain 1·3–1·5 wt % Na_2O and coexisting orthopyroxene has 0·2–0·4 wt % Na_2O, which appears to be a pressure effect on Na partitioning. In the olivine layers, interserts of quenched carbonate-bearing silicate melt were present in P86 and P85 whereas P84 contained small intergranular areas of quench dolomite. The first appearance of hydrous silicate melt (i.e. the solidus for water-rich vapour) is inferred to be ~1375°C at 6 GPa.

'Dry' experiments, water in NAMs and limits on pargasite stability

The experimental data correlating the added water contents with changing compositions of pargasite and clinopyroxene (Fig. 4) provide assurance that our experimental methods of controlling water content are effective in achieving relative differences between experiments. However, the presence of pargasite in 'dry' experiments at 1000°C in both HZ1 and HZ2 compositions shows that we are not able to completely eliminate water (hydrogen) by the experimental methods and run times (7 days) used, which yield a 'background' water content of ~0·1 wt % H_2O [~200 ppm in NAMs and ~750 ppm in pargasite, which corresponds to ~5% modal amphibole (Supplementary Data EA 4 and 5)]. We also note that pargasite did not occur in the 1100°C, 2·4 GPa, 3 days (O16) experiment on 'dry' HZ2 composition and that the pargasite in the 1050°C, 2·5 GPa (P78) experiment with 0·05 wt % H_2O has a high K_2O content (0·78 wt %), and thus the least modal pargasite (~4%) among the 2·5 GPa experiments with low water content. Although we are unable to completely eliminate water (hydrogen) from our experiments, Fig. 5 suggests that, at 2·5 GPa and 1000°C, pargasite is absent from HZ lherzolite at water contents below 100–150 ppm. For such low water contents, water resides only in NAMs. With increasing water content, modal pargasite increases to a maximum of ~7% at 2·5 GPa (P80) and water in NAMs increases to ~200 ppm (Kovács *et al.*, 2012) before an aqueous vapour phase appears (at ~1500 ppm bulk water content at 2·5 GPa). From ~1500 ppm to 5 wt % H_2O, the vapour phase increases and coexisting pargasite and clinopyroxene decrease in Na_2O and K_2O as these components dissolve in the vapour–fluid phase. Pargasite is unstable in lherzolites HZ1 and HZ2 at water contents >5 wt % as shown by our experiments and those of Grove *et al.* (2006) and Till *et al.* (2012*a*).

The chemical controls on pargasite stability include the activity of water and also the chemical activities of other oxide components. Thus the limits on pargasite stability determined for HZ1 and HZ2 compositions will differ slightly for other mantle compositions as already

demonstrated for the 'fertile' (MOR Pyrolite), 'enriched' (Hawaiian Pyrolite) and 'depleted' (Tinaquillo Lherzolite) compositions (Wallace & Green, 1991; Niida & Green, 1999). Chemical activity of water also controls the partitioning of water into NAMs and, when an aqueous vapour phase is present in a fertile lherzolite, the activity of water is reduced by other dissolved components (Ardia *et al.*, 2012; Kovács *et al.*, 2012; Tenner *et al.*, 2012; Gaetani *et al.*, 2014). Our experimental methods using monomineralic layers bounding the HZ1 lherzolite composition allowed measurement of the structurally bound water content of NAMs, particularly olivine, orthopyroxene and clinopyroxene, and of the partitioning of water between NAMs (Kovács *et al.*, 2012) in a model mantle lherzolite composition, including the role of minor carbonate.

DISCUSSION

Reconciliation of conflicting interpretations

Our experimental study demonstrates that the H_2O/Na_2O ratio of an experimental charge is an important factor in determining the phase relations of lherzolite, including the composition and abundance of quench films of silica-rich glass (Fig. 3). If the earlier studies quoted in the introduction are examined, it is apparent that in those in which H_2O/Na_2O was >150 (mol. ratio) the researchers inferred low solidus temperatures and pargasite breakdown at <2 GPa (Mysen & Boettcher, 1975; Grove *et al.*, 2006; Till *et al.*, 2012*a*). This interpretation was based on the observation of glass in experiments below 1000°C, but the distinction between glass from a vapour phase and glass from a hydrous melt phase was based on the expectation 'that a quenched fluid phase would produce spherical blebs of a SiO_2-rich component by unmixing from a dominantly fluid phase' (Grove *et al.*, 2006). No analyses of glass or of quench aggregates below 1000°C were obtained and glasses analysed from higher temperature experiments were silica-rich and low in Na_2O and CaO (Till *et al.*, 2012*a*). These inferred melt compositions were not tested for quench modification of initial melts, despite prior demonstration of this effect (Green, 1976), and the criticisms of these inferred melt compositions by Green *et al.* (2012) were not addressed by Till *et al.* (2012*b*). Although Till *et al.* (2012*a*) listed prior studies of water-saturated melting of lherzolite, they restricted their references (Till *et al.*, 2012*a*, table 3) to 'H_2O-rich' experiments and did not refer to studies documenting pargasite stability and melt compositions with bulk water contents of <5 wt % H_2O. The results from Grove *et al.* (2006) and Till *et al.* (2012*a*) should not be used as argument for production of silica-oversaturated melts by hydrous melting of lherzolite.

In contrast to the experiments with high H_2O/Na_2O, in studies with H_2O/Na_2O <50, all researchers (Kushiro *et al.*, 1968; Green, 1973*b*, 1976; Millhollen *et al.*, 1974; Wendlandt & Eggler, 1980; Mengel & Green, 1989; Wallace & Green, 1991; Niida & Green, 1999; Fumagalli *et al.*, 2009; Green *et al.*, 2010, 2011; Tumiati *et al.*, 2013) observed pargasite to higher pressures (2·5–3 GPa) and inferred solidus temperatures near 1000°C. The observations in the studies with high and low water contents are reconciled in Fig. 5, identifying the subsolidus NAMs + Vapour field for high water contents and the NAMs + Pargasite ± Vapour field for lower water contents. Almost all mantle scenarios involving magmatic activity, metasomatism or metamorphism (except those involving fluid flow through fractures or channels) envisage low H_2O/Na_2O around three or less.

The vapour-saturated solidus for fertile lherzolite HZ1 (model upper mantle)

In fertile lherzolite compositions, the amphibole pargasite is stable at the vapour-saturated solidus to pressures of 3 GPa. Chlorite does not occur at the vapour-saturated solidus of fertile lherzolite at any pressure. Glass observed at temperatures <1000°C is quenched from a vapour phase containing leached oxide components (particularly Na_2O and SiO_2) and is not indicative of a hydrous silicate melt. The data presented refute the interpretation that the vapour-saturated solidus of fertile lherzolite is at ~810°C at 3–6 GPa; that is, up to 800–900°C below the anhydrous solidus (Mysen & Boettcher, 1975; Grove *et al.*, 2006; Till *et al.*, 2012*a*).

Experiments with 0·145, 0·3 and 1·45 wt % H_2O define the vapour-saturated solidus at 2·5, 4 and 6 GPa and at each P there is a clear distinction between above-solidus experiments in which interserts of quench amphibole, oxide and carbonate aggregates are present in the olivine layers, and subsolidus experiments in which such interserts are absent. The melt fraction that segregated into olivine melt-trap layers in experiments near the solidus is from 1 to 5 modal % of the HZ lherzolite composition. Subsolidus experiments are porous and contain very small iron-enriched carbonate or carbonate + oxide areas. These are interpreted as quenched carbonatite melt (resulting from inability to exclude trace carbon from experiments) accompanying water-rich vapour.

The solidus marking the appearance of hydrous silicate melt in lherzolite HZ1 composition decreases in T with increasing P to a minimum of ~970°C at 1·5–2 GPa, and then increases to ~1010°C at 2·5 GPa, ~1210°C at 4 GPa, and ~1375°C at 6 GPa (Fig. 6). Although there is evidence that the aqueous vapour phase contains increasing solute components with increasing P, our experiments show the appearance of quenched hydrous silicate melt over a small temperature interval rather than a gradual increase in silicate/carbonate over a larger temperature interval; that is, we do not find evidence for supercritical behaviour in HZ1 lherzolite at 6 GPa or lower pressure. In addition, as a potential second critical endpoint is approached in P–T

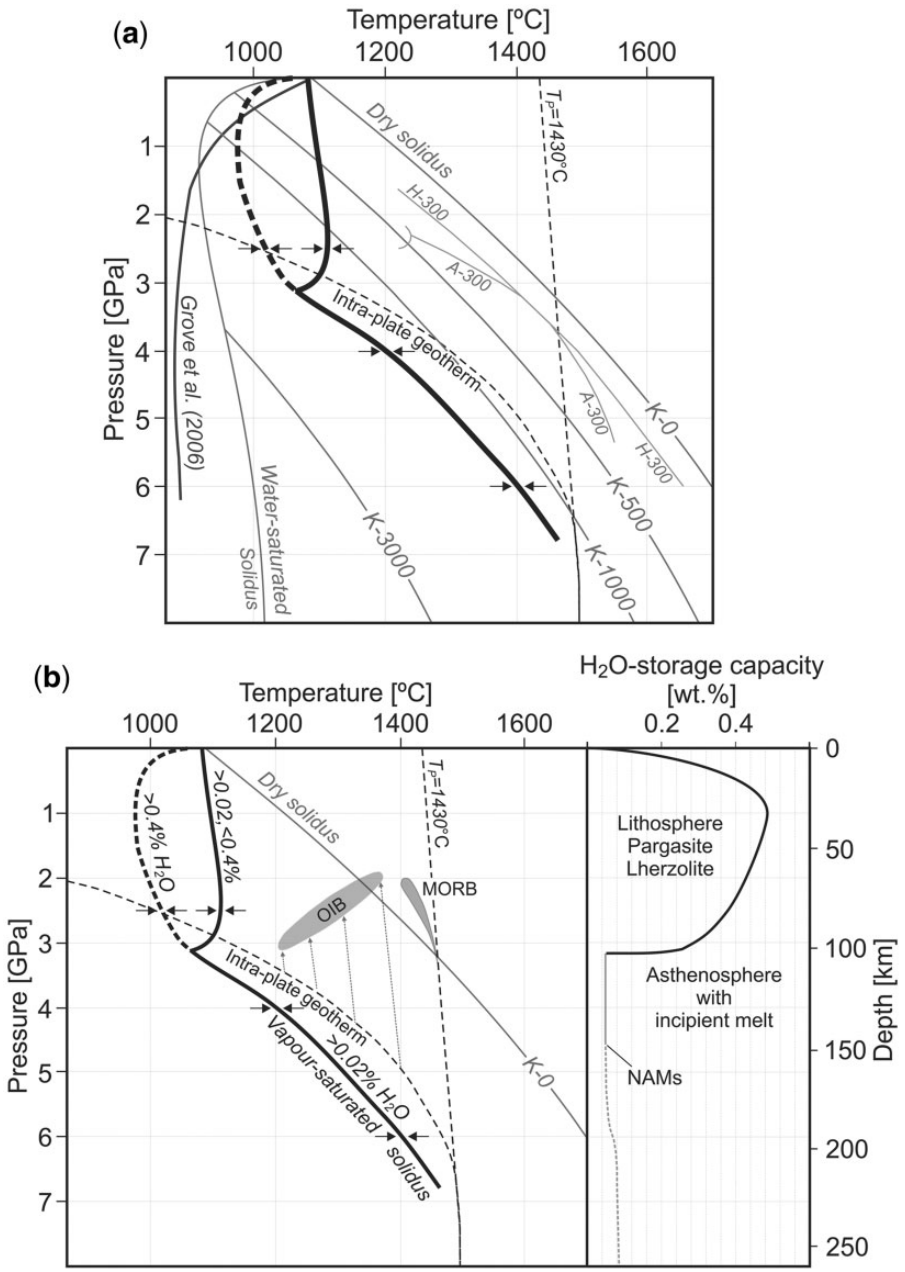

Fig. 6. (a) Comparison of experimentally determined solidus for hydrous silicate melt in fertile lherzolite with several recent model solidi for different water contents. Bold black line is the experimental solidus for >200 ppm H_2O. At >3 GPa it is the vapour-saturated solidus as a maximum of ~200 ppm H_2O is held in NAMs [right-hand panel of (b)]. At <3 GPa it is the solidus for pargasite-bearing lherzolite with subsolidus water stored in pargasite and NAMs, for mantle water contents from 200 to 4000 ppm. The vapour-saturated solidus is shown by the bold dashed line. Arrows indicate experimental determination of the solidus at 2·5, 4 and 6 GPa. Thinner black line labelled Grove *et al.* (2006) is the inferred water-saturated solidus (14·5 wt % H_2O) from Grove *et al.* (2006) and Till *et al.* (2012a). Fine grey lines labelled Water-Saturated Solidus, K-3000, K-1000, K-500 and K-0 are from Katz *et al.* (2003) and are the solidus for water-saturated conditions [based on preliminary data from Grove *et al.* (2006) experiments], and calculated solidi for 3000 ppm, 1000 ppm, 500 ppm and zero H_2O respectively. The latter are based on assumed high solubility of water in NAMs (e.g. ~3000 ppm H_2O at 4 GPa, 1000°C). The lines labelled H-300 and A-300 are the calculated solidi for 300 ppm H_2O of Hirschmann (2006) and Asimow *et al.* (2004) respectively. Our experimental study, including the companion paper detailing the measurement of water in NAMs (Kovács *et al.*, 2012), suggests that modelled solidi H-300, A-300, K-500, K-1000 and K-3000 should lie on the experimental vapour-saturated solidus at >3 GPa. A model intraplate geotherm and mantle adiabat for mantle potential temperature of 1430°C (Green *et al.*, 2001) are shown as dashed lines. (b) Panel at right plots the water storage capacity of fertile, MORB-source mantle as a function of depth along the vapour-saturated solidus. At <100 km approximately pargasite is stable to the solidus but the modal abundance of pargasite reaches a maximum at 1–1·5 GPa and decreases towards higher pressure (Niida & Green, 1999), hence the water storage capacity decreases with modal pargasite. Pargasite becomes unstable at >3 GPa, and water storage capacity drops to that (~200 ppm) which can be retained in NAMs in fertile lherzolite. Panel at left shows experimentally determined solidi, intraplate geotherm and mantle adiabat as in (a). The intraplate geotherm intersects the mantle dehydration solidus (pargasite-bearing lherzolite) at ~90 km and at deeper levels a small melt fraction is present if water contents are >200 ppm, providing an explanation for the asthenosphere and lithosphere–asthenosphere boundary. The geotherm is shown joining the mantle adiabat at 200–250 km and the depth interval from 90 to 250 km

(continued)

space the concentrations of water in silicate melt (c_{melt}) and in the vapour phase (c_{vapour}) should converge ($c_{melt}/c_{vapour} \sim 1$). The contrasted nature of the quench aggregates above and below the inferred solidus, their modal abundance and compositions do not suggest such convergence. Our experiments on HZ1 lherzolite and HZ1 +5% phlogopite (Supplementary Data EA 9) provide further information on the different behaviour of K_2O and Na_2O. Although they are similar in their role in melting up to ~2·5 GPa, with increasing pressure (i.e. including the breakdown of pargasite above ~3 GPa), K_2O is increasingly incompatible, whereas Na_2O is increasingly compatible in clinopyroxene. Thus, although both partition strongly into an aqueous vapour phase, the proportion of K_2O partitioned into a vapour phase towards greater mantle depths is considerably higher than that of Na_2O.

The most important aspect of our new data is the confirmation of earlier experiments showing that the vapour-saturated solidus in fertile lherzolite + H_2O is a minimum at 1·5–2 GPa and has positive dT/dP at higher P (Fig. 6). There is a clear distinction between hydrous silicate melt (~30 wt % H_2O) above the solidus and aqueous vapour below the solidus. At pressures >2·5–3 GPa, the anhydrous and vapour(water)-saturated solidi are roughly parallel in P–T space with aqueous vapour-saturation depressing the solidus by ~350°C at 5–6 GPa (see also Tenner *et al.*, 2012).

In Fig. 6a we compare the experimental determination of the effect of water on melting of a model mantle composition with several models (Katz *et al.*, 2003; Asimow *et al.*, 2004; Hirschmann, 2006; Hirschmann *et al.*, 2009) that infer high water solubility in NAMs and use partitioning of water between NAMs and melt to predict the mantle solidus depression as a function of mantle water content. Katz *et al.* (2003) used a low-temperature water-saturated solidus based on preliminary data subsequently published by Grove *et al.* (2006). They predicted water-undersaturated solidi for 500, 1000 and 3000 ppm H_2O as parallel to the dry solidus. Thus the predicted solidus for mantle water contents of 3000 ppm H_2O is depressed by ~550°C at >4 GPa and that for 1000 ppm is depressed by ~250°C at >0·6 GPa. For smaller water contents of 500 ppm or less, an intraplate geotherm would not intersect the solidus before meeting the mantle adiabat ($T_p = 1430$°C) and upwelling mantle at $T_p = 1430$°C would begin melting at ~150 km depth.

Asimow *et al.* (2004) calculated a water-saturated solidus ($a_{H2O} = 1$) with a positive dT/dP at >0·2 GPa, roughly parallel to the anhydrous solidus, and included a stability field for amphibole below 2·7 GPa. The predicted solidus for 300 ppm H_2O is plotted in Fig. 6a and is close to the interpolated position of the 300 ppm solidus of Katz *et al.* (2003) at 2·5 and 5 GPa but shows lower solidus depression at 3–4 GPa.

Hirschmann (2006) and Hirschmann *et al.* (2009) predicted solidi for 50, 200, 300 and 1000 ppm H_2O [i.e. values modelling MORB-source mantle (50–200 ppm) and ocean island basalt (OIB)-source mantle (300–1000 ppm)]. The predicted solidi are parallel to the dry solidus and thus also to the Katz *et al.* (2003) solidi but with smaller solidus depression for a given water content. All three models are based on the premise that the water contents appropriate to the upper mantle (MORB-source or OIB-source) can be retained in NAMs at subsolidus conditions. Our experimental study defines limits to water contents in NAMs and the role of pargasitic amphibole in increasing water storage capacity at <3 GPa. At 2·5–4 GPa the limit to water solubility in NAMs is ~200 ppm and for any water contents >200 ppm, the mantle at >3 GPa is vapour-saturated and the solidus is as plotted in Fig. 6a and b. The solidus depression for 200 ppm H_2O at >3 GPa is much greater than predicted by all four models (i.e. Katz *et al.*, 2003; Asimow *et al.*, 2004; Hirschmann, 2006; Hirschmann *et al.*, 2009) but water contents greater than 200 ppm do not result in further solidus depression. Larger water contents result in more water-rich vapour below the solidus or melt ± vapour at the solidus and increased melt fraction above the solidus. If the upper mantle contains more than 200 ppm H_2O the P–T field between vapour-saturated and dry solidi may be contoured for melt fraction (Green & Falloon, 2005, fig. 3A and B) using an empirical relation between water content and liquidus depression for olivine-rich magmas (Fig. 1). If the upper mantle contains less than 200 ppm H_2O the position of the solidus within the P–T field between vapour-saturated and dry solidi may be mapped using a modified modelling approach, as in the studies by Katz *et al.* (2003), Asimow *et al.* (2004), Hirschmann (2006) and Hirschmann *et al.* (2009). We emphasize that the very low temperatures inferred for the vapour-saturated mantle solidus by Katz *et al.* (2003), Grove *et al.* (2006) and Till *et al.* (2012*a*) are incorrect and the maximum solidus depression owing to water in the mantle is ~350°C at 2·5–3 GPa.

Fig. 6. Continued
is one in which a very small, near-solidus melt may migrate along the geotherm, enriching the upper asthenosphere and depleting the lower asthenosphere in incompatible elements. MORB are shown as sourced from upwelling lower asthenosphere (i.e. source lherzolite with ~200 ppm H_2O, and depleted LREE and LILE element abundances), with melt fraction increasing rapidly above the anhydrous solidus and melt segregation at ~15–20% melting at ~2 GPa. Intraplate basalts, including OIB, are shown as the products of upwelling of enriched lherzolite from the middle and upper asthenosphere, with source water and incompatible element contents increasing with decreasing depth and temperature of upwelling. Intraplate magmas range from olivine melilitites and nephelinites at deeper levels and smaller melt fraction, to olivine tholeiites at higher melt fraction and higher temperatures [see text and also Green & Falloon (1998, 2005)].

The vapour-undersaturated solidus (dehydration solidus) for fertile lherzolite (HZ1)

Pargasite is stable at the vapour-undersaturated solidus of HZ1 lherzolite at 2·5 GPa. The solidus for hydrous silicate melt is a cotectic melting of pargasite lherzolite in which vapour either is absent or has low water activity because of dissolved oxide components or carbon species (e.g. CH_4, CO_2). The solidus T is ~1100°C and is almost independent of pressure between 0·2 and 2·5 GPa. It has strongly negative dT/dP at 2·8–3 GPa and intersects the vapour-saturated solidus close to 3 GPa, 1010°C (Fig. 6b). The stability, composition and modal abundance of pargasite are controlled by bulk composition (including water), P and T, and f_{O2} (Green, 1973*b*; Taylor & Green, 1988; Wallace & Green, 1988; Niida & Green, 1999; Green *et al.*, 2010; this study). The vapour-undersaturated solidi for lherzolites also differ for different bulk compositions. The variations in modal abundance and composition of pargasite with P and T observed in this study of HZ1 lherzolite are closely similar to those presented in the extensive study of the model mantle composition MOR Pyrolite (Niida & Green, 1999). Significant difference lies only in the K_2O content of pargasite in HZ1, compared with its absence in the MOR Pyrolite composition (Table 1).

The T maxima on pargasite lherzolite solidi are sensitive to bulk composition and increase from the most refractory composition (Tinaquillo Lherzolite) to the most enriched (Hawaiian Pyrolite) because of the role of the components Na, Ti, and K in stabilizing pargasite to higher T. Also, for a given bulk composition, the composition and modal proportion of pargasite at the solidus change with increasing P and T (Niida & Green, 1999; Green *et al.*, 2010; this study). Thus, the pargasite on the dehydration solidus at 1 or 1·5 GPa is more abundant but less sodic and with lower TiO_2 than pargasite on the solidus at 2·5–3 GPa. Pargasite may persist immediately above the solidus and the melt fraction and melt composition will vary with P and T. Melt fraction along the dehydration solidus can be estimated from the water available from modal pargasite, combined with an estimation of the water content of a primitive hydrous basalt with liquidus T at the P and T of interest; that is, from knowledge of the liquidus depression as a function of water content in olivine-rich magmas.

Melt compositions are generically alkali-rich and increasingly olivine-rich and silica-undersaturated with increasing pressure (i.e. towards deeper mantle levels). Based on normative compositions, in this study of HZ1 lherzolite, melt compositions at the solidus at 2·5 GPa with low water contents (melt fraction ~1–1·5%) are transitional between carbonatite and olivine melilitite, whereas at melt fraction of 2–6% the melt composition is olivine nephelinite to olivine-rich basanite (Supplementary Data EA 4, P79, O77; EA 5, O53).

At P–T conditions within the pargasite lherzolite stability field, subtle changes in P–T or water content can affect modal proportions of pargasite and thus the activity of water and the presence or absence of hydrous melt. For example, a fertile lherzolite at 2 GPa, 1050°C with ~12% pargasite contains ~2500 ppm water but is below the dehydration solidus (Fig. 6b). Access of additional water cannot be accommodated by additional pargasite but instead leads to melting as these P–T conditions are above the vapour-saturated solidus (Fig. 6b). The residue contains only the water content held in NAMs. This example illustrates a P–T window in which pargasite lherzolite can undergo melting isothermally and isobarically due to access of additional aqueous vapour phase.

In a second example, a lherzolite that has a small melt fraction at 1050°C, 3·2 GPa will freeze if it follows a near-adiabatic, upwelling path, and will show increasing modal pargasite with decreasing pressure (Fig. 6b). This freezing of melt on upwelling is a consequence of the negative dT/dP of the vapour-undersaturated solidus of fertile lherzolite at ~3 GPa, and is an exception to the general situation for anhydrous lherzolite in which near-adiabatic upwelling leads to melting. The converse is true for a lherzolite experiencing downwelling or subduction at pressures >1·5 GPa (Fig. 6b). Increasing P decreases the maximum modal pargasite and may release water and initiate melting with little change in T. These examples lead to the emphasis on the role of pargasite in the concept of water storage capacity for a model mantle composition.

The water storage capacity of fertile lherzolite

The water storage capacity of the model mantle composition may be defined as the amount of water that is held as structurally bound water in stoichiometric proportions in hydrous minerals stable at the P–T of interest, together with that held in solid solution in crystal lattices of NAMs. The water storage capacity of a particular chemical composition is a function of the relevant phase assemblage; that is, the stable mineralogy at the P and T of interest. The water storage capacity, thus defined, is a useful indicator of whether an aqueous vapour phase, hydrous silicate melt or supercritical water-rich fluid will be present for a given lherzolite composition and water content. In fertile or enriched lherzolite compositions such as MOR Pyrolite, HZ1 lherzolite or Hawaiian Pyrolite, presented as model compositions for upper mantle acting as a source for MOR basalts and 'hotspot' basalts respectively, the amphibole pargasite and the mica phlogopite are stable to solidus temperatures even in the presence of very small amounts of water. Pargasite, however, is unstable at pressures greater than 3 GPa and phlogopite occurs only if K_2O contents are enriched above those appropriate for MORB-source compositions (Green, 1973*b*; Mengel & Green, 1989; Konzett & Ulmer, 1999). Thus the water

storage capacities of inferred mantle compositions are sensitively dependent on the stabilities of hydrous phases (i.e. on bulk composition, *P* and *T*).

In the model mantle compositions HZ1 and MOR Pyrolite there are higher modal contents of pargasite at subsolidus conditions at 1·5 GPa than at 2·5 GPa (Supplementary Data EA 4 and 5; Niida & Green, 1999; Green *et al.*, 2010; this study). Pargasite and coexisting phases have very similar compositions at similar temperatures in the two compositions (HZ1 and MOR Pyrolite) and the lower modal abundances of pargasite in HZ1 lherzolite than in MOR Pyrolite are attributed to the higher Na_2O content of the latter (Table 1). The water storage capacity of HZ1 lherzolite decreases from ~3000 ppm at 1·5 GPa (15% pargasite) to ~1500 ppm (7% pargasite) at 2·5 GPa as the modal pargasite changes as a function of *P*. It then drops abruptly to ~200 ppm at ~3 GPa as pargasite is destabilized by *P* (Fig. 6b). If MOR Pyrolite rather than HZ1 lherzolite is used as the inferred composition for the upper mantle (MORB-source) then these water storage capacities would be *c.* 3800 ppm (18% pargasite) and 2600 ppm (12% pargasite) at 1·5 and 2·5 GPa respectively (Niida & Green, 1999, figs 6 and 8).

Pargasite is unstable at and below the lherzolite + H_2O vapour-saturated solidus at pressures >3 GPa in the fertile (HZ1, MOR Pyrolite) and enriched (Hawaiian Pyrolite) compositions and >2·6 GPa in the depleted lherzolite composition (Tinaquillo Lherzolite). In all cases the water storage capacity decreases to that which can be held in NAMs. In the studies by Kovács *et al.* (2012) and Green *et al.* (2010, 2011) the water storage capacity at the vapour-saturated solidus was shown to be ~200 ppm H_2O at 2·5 and 4 GPa. Our data show that, for model mantle compositions proposed as source composition for generating MORB by near-adiabatic upwelling at mid-ocean ridges, if water contents exceed ~200 ppm, then at subsolidus conditions an aqueous vapour phase is present and melting begins at the vapour-saturated solidus. Melt compositions are highly alkaline, silica-undersaturated and olivine-rich and, in the presence of trace carbon contents, transitional between olivine melilitites and carbonatites.

The measurement of water contents in NAMs at and above the vapour-saturated solidus, together with studies showing maximum water solubility of ~25–30 wt % H_2O in olivine-rich mantle-derived magmas (Fig. 1), leads us to estimation of the bulk H_2O peridotite/melt partition coefficient $D_{H_2O}^{peridotite/melt}$ of ~0·0006 (Green *et al.*, 2010; Kovács *et al.*, 2012). This value is lower than inferred or measured in other studies, such as those by Hauri *et al.* (2006), Hirschmann *et al.* (2009), and Ardia *et al.* (2012). The low value is a consequence of low water concentrations in olivine and pyroxene (Kovács *et al.*, 2012) and the high water contents necessary to depress the liquidus of olivine-rich melts to the temperatures of the vapour-saturated solidus at 2·5–4 GPa. However, $D_{H_2O}^{peridotite/melt}$ depends on mineral composition, *P*, *T*, and melt compositions as demonstrated in the above-mentioned studies. At subsolidus conditions the water-rich vapour phase carries solute components (including Na_2O, K_2O, SiO_2), and volatiles CO_2–CH_4, which lower the activity of water and influence the particular defect site for H_2O entry in minerals. We thus consider that our empirical method using mantle lherzolite to control phase assemblages and compositions, including melt and/or vapour phases, and monomineralic 'sensor' layers of NAMs, is an effective approach to understanding the issues around water storage and incipient melting in the upper mantle. Ardia *et al.* (2012) adopted this approach using a lherzolite composition (KLB-ox) that is also similar to HZ1, exploring melt–residue relations at 5–8 GPa, 1400–1500°C. Bulk water contents were 0·5, 0·75 and 1 wt % H_2O and water contents in NAMs were measured by secondary ionization mass spectrometry (SIMS). Conditions are well above the vapour-saturated solidus and residues were lherzolite or garnet harzburgite. Melt compositions could not be determined and estimation of water contents in melts as 4·5–13 wt % rely on inferred values of $D_{H_2O}^{mineral/melt}$. The measured water contents in NAMs, particularly olivine, are higher than those of Kovács *et al.* (2012), although there is some convergence at lower pressures (5 GPa). However, the lowest water content in olivine (57 ± 26 ppm) is at 1450°C, 5 GPa with a bulk water content of 0·5 wt %, so that the melt is vapour-undersaturated and water activity lower than at solidus conditions (Ardia *et al.*, 2012). From their study, Ardia *et al.* (2012) considered that water contents of ~200 ppm in the MORB source are insufficient to cause melting along the mantle intraplate geotherm as we propose. However, this is based on an assumed $D_{H_2O}^{peridotite/melt}$ that is higher than that which we have found at the vapour-saturated solidus. We note the presence of carbonate in our experiments so that the activity of water is lowered and $D_{H_2O}^{peridotite/melt}$ may be modified. It is pertinent that in the upper mantle and magmas derived therefrom, both water and CO_2 are present and unavoidably interact, particularly through redox reactions (Taylor, 1985; Green *et al.*, 1987; Taylor & Green, 1988; Foley *et al.*, 2009; Stagno & Frost, 2010; Foley, 2011; Dasgupta *et al.*, 2013; Stagno *et al.*, 2013).

APPLICATIONS TO MAGMA GENESIS AND GEODYNAMICS

The nature of the asthenosphere and the lithosphere–asthenosphere boundary

Experimental petrology maps the mineralogy, the melting behaviour and the presence or absence of a vapour phase as functions of *P*, *T*, and bulk composition. Physical properties (rheology, seismic velocity and electrical conductivity) attributable to the phase fields and boundaries define the

asthenosphere and the lithosphere–asthenosphere boundary (LAB), the low-velocity zone (LVZ) and electrically conductive layer (ECL) respectively. This study of HZ lherzolite + H_2O (including the role of minor CO_2) coupled with prior studies of MOR Pyrolite and Hawaiian Pyrolite + (C–H–O) contributes to possible explanations for these upper mantle layers and boundaries. The data from parental MORB, intraplate basalts, and mantle-derived peridotites are in favour of $H_2O > CO_2$ in the upper mantle (Michael, 1995; Danyushevsky *et al.*, 2000; Dixon & Clague, 2001; Saal *et al.*, 2002). It is also argued that mantle fO_2 decreases with increasing depth (O'Neill & Wall, 1987; O'Neill *et al.*, 1993; Ballhaus, 1995; Gudmundsson & Wood, 1995; Rohrbach *et al.*, 2007; Frost & McCammon, 2008; Rohrbach & Schmidt, 2011; Stagno *et al.*, 2013) to stabilize graphite–diamond and H_2O-rich fluid, and that $H_2O + CO_2$ vapour or carbonate minerals are stable only in the uppermost mantle (<~2–3 GPa) (except in subducted slab or mantle wedge settings). Explanations for the existence of the asthenosphere, the LVZ and ECL may lie in the intersection of inferred geothermal gradients with the phase fields and boundaries appropriate to the upper mantle composition.

The P–T conditions for carbonatite melt in intraplate settings have been demonstrated experimentally (Wyllie, 1978, 1979; Wallace & Green, 1988; Dasgupta & Hirschmann, 2006) and evidence for the migration and decarbonation of carbonatite melts in the lithosphere (~1·5 GPa) has been documented in spinel lherzolite xenolith suites from continental intraplate settings (e.g. Yaxley & Green, 1996; Scott *et al.*, 2014). Provided that the mantle from ~1·5 to 3 GPa is sufficiently oxidized, an intraplate geotherm may traverse the field of sodic, dolomitic carbonatite melt with pargasite-bearing spinel or garnet lherzolite [as illustrated in figs 7.6 and 7.8 of Green & Falloon (1998)]. In this case the melt fraction will be approximately twice the CO_2 content (i.e. ~0·08% melt for a mantle CO_2 content of 400 ppm). It is possible that the low viscosity of carbonatite melt, high permeability, and the nature of the decarbonation boundary with consequent CO_2 degassing combine to make the carbonatite + pargasite lherzolite field a transient or ephemeral phenomenon. The most appropriate geophysical method to detect this field and its upper boundary may be electrical conductivity (Gaillard *et al.*, 2008; Sifré *et al.*, 2014). Investigation should be focused on areas of lithospheric thinning and recent intraplate volcanism such as SE Australia, South Island, New Zealand, and Eifel and the Rhine Graben in Europe, where the decarbonation reactions in mantle xenoliths have been recognized.

Focusing attention on upper mantle compositions represented by the global MORB-source mantle, or modern, well-mixed upper mantle (i.e. compositions close to HZ1 lherzolite or MOR Pyrolite), then estimated geothermal gradients in regions of mature oceanic and young continental lithosphere intersect the mantle solidus and pargasite breakdown reaction (Fig. 6). Such geotherms pass from subsolidus to partially molten lherzolite at ~90 km depth, provided that the upper mantle contains >200 ppm H_2O. Recent work (Faul & Jackson, 2007) on mantle rheology demonstrates that very small degrees of partial melting have a marked effect on dunite rheology, increasing strain rates by two orders of magnitude. It is argued that the most plausible explanation for the rheological contrast between lithosphere and asthenosphere is the transition along the geotherm from subsolidus pargasite lherzolite to partially molten garnet lherzolite, the melt fraction present being determined primarily by the water content (Lambert & Wyllie, 1970; Green, 1971, 1972; Green & Falloon, 1998, 2005; Niu & O'Hara, 2009; Green *et al.*, 2010, 2011).

Our data are also relevant to the suggestion (Hirth & Kohlstedt, 1996) that the asthenosphere is subsolidus, water-bearing mantle and is rheologically weak because of intracrystalline water, particularly in olivine. In this model the overlying lithosphere is inferred to be 'dry', having lost intracrystalline water into a melt phase in the upwelling and melt extraction involved in lithosphere formation at MOR settings (Hirth & Kohlstedt, 1996). Lithosphere formation at MOR settings is a high-T process in which low water contents in MORB and partitioning of water into residual NAMs is expected to yield 'dry' residues (≪200 ppm H_2O). With aging of the lithosphere, access of water results in the appearance of the hydrous phase pargasite when activities of components entering pargasite, particularly Na_2O, TiO_2, K_2O and H_2O, are sufficiently high (Bonadiman *et al.*, 2014). In Fig. 5 the appearance of pargasite at 2·5 GPa, 1000°C is estimated to occur at ~150 ppm H_2O; that is, less than that which can be held in NAMs (~200 ppm). High strength or rigidity of the lithosphere is a consequence of absence of melting and retention of water in both NAMs and pargasite (and phlogopite in the presence of excess potassium). As our data show, the water content in residual NAMs at the vapour-saturated solidus changes little across the solidus (Kovács *et al.*, 2012). We suggest that lower viscosity in the asthenosphere is not due to higher water content in NAMs but to the presence of incipient melt in mantle with >200 ppm H_2O at P >3 GPa.

A near-solidus migratory melt fraction cannot ascend above ~90 km by porous flow along the geotherm, as it reacts and freezes as pargasite (and phlogopite in the presence of excess potassium) in lithospheric lherzolite or harzburgite. There is thus a natural 'lid' to the asthenosphere or incipient melting region at ~90 km depth (see Rychert & Shearer, 2011). This depth is stable through ~100°C of cooling of the intra-plate geotherm because of the P–T shape (large negative dT/dP) of the lherzolite dehydration solidus. There is also a depth interval along the geotherm

where rising incipient melts may pond; that is, they are unable to ascend either by porous flow or mantle upwelling because of intersection with the pargasite stability field. This may produce a melt-rich channel at ~90 km depth.

The phase assemblages and boundaries defined by the experimental studies also determine seismological properties and it is commonly inferred that the seismic LVZ equates to the asthenosphere and that seismological observations can be used to characterize the depth and boundaries of the asthenosphere. In their paper on seismological evidence for Pacific Ocean lithospheric thickness, Rychert & Shearer (2011) inferred that the lithosphere–asthenosphere boundary corresponds to an isotherm at 930°C with a 95% confidence from 820 to 1020°C; that is, an upper limit close to the solidus of fertile lherzolite at 3 GPa. They noted that in some areas the sharpness of the lithosphere–asthenosphere boundary implies a mechanism other than increasing temperature alone. Rychert & Shearer (2011) suggested that the imaged boundary may be a permeability boundary, with a small amount of partial melting below it. The experimental studies of pargasite in lherzolite have provided an explanation for such a feature at ~90 km depth and 1000–1100°C (Green & Liebermann, 1976). Other studies (Thybo & Perchuc, 1997; Thybo, 2006; Fischer *et al.*, 2010; Kind *et al.*, 2012) inferred that the top of the LVZ is at ~100 km depth beneath stable oceanic crust, but a shallower depth (50–70 km) has also been inferred (Schmerr, 2012). If the petrological arguments for explanation of the LAB (and possibly the top of the LVZ and ECL) as the intersection of the geotherm with the solidus of pargasite lherzolite are correct, then the lithosphere will cool and thicken to ~90 km (at ~1100°C) with increasing distance from mid-ocean ridges and remain approximately at this depth for further cooling of ~100°C (reflecting the steep negative dT/dP at ~3 GPa) before thickening with further cooling (intersection of geotherm and vapour-saturated solidus at >3 GPa). These predictions may be tested, particularly by seismological and electrical conductivity studies.

Application to intraplate magmatism

Our new experimental study continues a theme of experimental melting studies of lherzolite + (C, H, O) and the inverse approach to find the P, T, H_2O, CO_2, conditions for which the minerals olivine + orthopyroxene ± clinopyroxene ± garnet ± Cr/Al-spinel occur on or close to the liquidi of primary intraplate magmas. This model for intraplate mantle melting was summarized by Green & Falloon (2005, figs 2 and 3), and is shown in a simplified form in Fig. 6b. In the model the P–T field between the vapour-saturated solidus and the anhydrous solidus is contoured for melt fraction and water content of the hydrous silicate melt. Two different volatile (H_2O, CO_2) contents, modelling MORB and intraplate basalt sources respectively, were considered and it was assumed that ~100 ppm H_2O was retained in NAMs. Applying our new data to these models, the water in residual NAMs should be ~200 ppm and the models of fig. 3A and B of Green & Falloon (2005) relabelled as '300 ppm H_2O' and '1100 ppm H_2O' respectively. These models are illustrations of the consequence of incipient melt migration through the asthenosphere along the geotherm. It is suggested that this continuously evolves contrasted 'enriched' and 'depleted' reservoirs. The reservoirs are represented by garnet lherzolite and added melt (<2% approximately) in the upper part of the asthenosphere, and garnet lherzolite (~200 ppm H_2O) with a vanishingly small melt fraction in the lower part of the asthenosphere.

If thinning of the lithosphere occurs, then upwelling of the upper asthenosphere increases the melt fraction and may lead to melt segregation. Melt extraction from upwelling upper asthenosphere yields the spectrum of intraplate, mantle-derived (particularly xenolith-bearing) magmas from olivine melilitite to olivine tholeiite, including enriched (E)-MORB (Fig. 6b). This model is consistent with the inverse approach to mantle melting in which mantle-derived parental magmas (selected on the basis of hosting lherzolite xenoliths and having Mg# ~75) have been investigated by experiment to establish the P, T, H_2O and CO_2 contents at which they have olivine + orthopyroxene ± clinopyroxene ± garnet ± Cr/Al-spinel on or close to their liquidi. These inverse experimental studies (e.g. Green & Ringwood, 1967; Green & Hibberson, 1970; Green, 1973*a*; Brey & Green, 1977; Foley, 1989; Eggins, 1992*a*, 1992*b*) established the relationships between P, T, and melt fraction summarized in Fig. 6b and by Green & Falloon (2005). The major element compositions (normative mineralogy) of parental magmas are constrained by the coexisting residual mineralogy (i.e. by phase equilibria and consequent element partitioning). H_2O and CO_2 both play an essential role as highly incompatible components essential for generation of low-temperature, low-degree partial melts (Fig. 7). A further test of the model for intraplate magmatism summarized in Fig. 6b was provided by Frey *et al.* (1978), who examined the major and trace element compositions of olivine melilitites to quartz tholeites in the intraplate SE Australian Tertiary to Recent volcanic province. Using the constraints provided by the experimental determination of conditions for residual garnet lherzolite to spinel harzburgite mineralogies and measured partition coefficients for mineral/melt partitioning, those researchers concluded that 'a source pyrolite composition differing only' (from the Hawaiian Pyrolite composition) 'in having 0·3–0·4% TiO_2 rather than 0·7% TiO_2, is able to yield the spectrum of primary basalts for the Victorian–Tasmanian province by ~4 to ~25% partial melting' (Frey *et al.*, 1978).

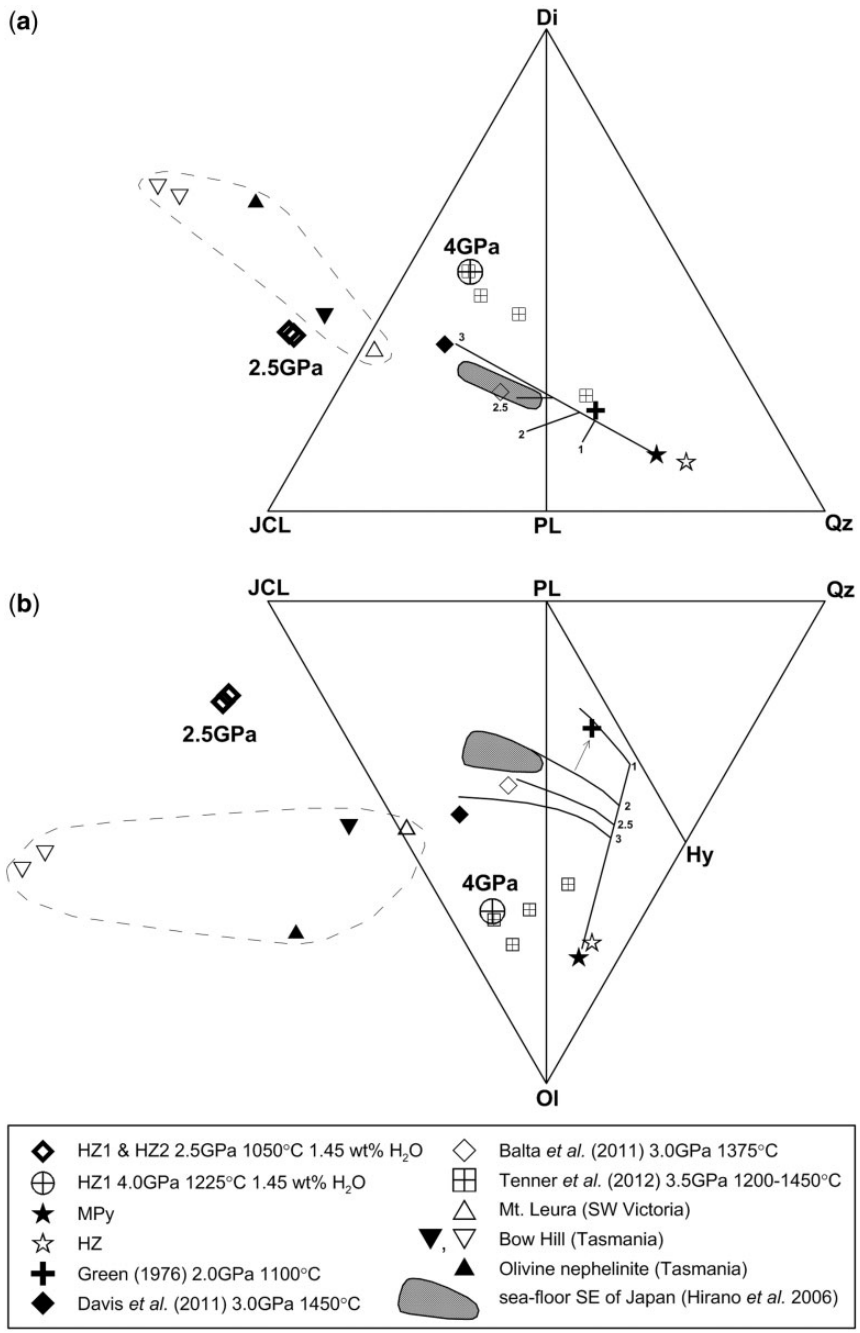

Fig. 7. (a, b) Compositions of experimentally determined near-solidus melts from HZ1 and HZ2 lherzolites plotted in the 'basalt tetrahedron'. Molecular proportions of oxides are cast into components SiO_2, $(Mg,Fe)_2SiO_4$, $Ca(Mg,Fe)Si_2O_6$ and $[(Na,K)AlSi_2O_6 + CaAl_2SiO_6]$. The diagram illustrates the degree of silica-saturation and diopside content in cotectic melting trends from lherzolite to dunite residue. The melt compositions from this study are compared with the dry melting trends for the MPy (MORB Pyrolite) composition (Falloon & Green, 1988) at 1–3 GPa. At 2 GPa water shifts the melt composition away from olivine towards a more silica-saturated and plagioclase-rich composition (Green, 1976). The near-solidus melt ('incipient melt') at 3 GPa, 1450°C, 'dry', from Davis *et al.* (2011) is consistent with the trend established for MPy. At 3 GPa, 1375°C a melt containing ~5 wt % H_2O with a garnet lherzolite residue is consistent with water causing a higher melt fraction and an expansion of the olivine field (Balta *et al.*, 2011). The vapour-saturated melt composition at 4 GPa, 1225°C is less silica-undersaturated but much richer in olivine and diopside than the 2·5 GPa melts. It overlaps with the most water-rich melt (23% H_2O) at 3·5 GPa, 1200–1450°C of Tenner *et al.* (2012). These melts lie on a harzburgite residue trend towards the olivine + melt control line. To compare the experimental melts with natural mantle-derived melts (see text) we have plotted examples (triangles) from the Tasmanian and SW Victorian Tertiary basalt province (Frey *et al.*, 1978). These have been experimentally shown to have Ol + Opx + Cpx + Ga saturation at 2·5–3 GPa, ~1150–1200°C with appropriate $CO_2 + H_2O$ contents (Green, 1973*b*; Adam, 1990). The field of the most magnesian alkali olivine basalts from very young intraplate volcanoes from the sea-floor SE of Japan is also shown (Hirano *et al.*, 2006). Ol, olivine; Qz, quartz; Di, diopside; Hy, hypersphene; Pl, Ab + An + Or (Ab, albite; An, anorthite; Or, orthoclase). JCL, Jd + CaTs + Lc (Jd, jadeite; CaTs, Ca-Tschermaks; Lc, leucite).

At low melt fractions, melt compositions, particularly the abundance of incompatible elements, are very sensitive to source composition, melt fraction and stability of garnet and minor phases such as phlogopite, apatite, and ilmenite in the residue. Our experimental data provide estimates of near-solidus melts (1–5% melt fraction) at 2·5 GPa (Supplementary Data EA 4, P79, O77; EA 5, O53) and at 4 GPa (Supplementary Data EA 4, O98) and 6 GPa (Supplementary Data EA 4, P49). The melts at 2·5 GPa are consistent with earlier liquidus studies at 2–3 GPa on primitive olivine-rich basanites, nephelinites, melilitites, mugearites and carbonatites including the roles of H_2O and CO_2. This is illustrated in Fig. 7, where the melt compositions at 1050°C, 2·5 GPa plot in the field of mantle-derived olivine-rich basanites to nephelinites for which 'inverse' experimental studies have established conditions of lherzolite saturation, requiring both H_2O and CO_2 in the source.

Our calculated melts at similar melt fraction (<5%) at 4 and 6 GPa show increasing CaO and MgO and decreasing SiO_2, Al_2O_3, and Na_2O from 2·5 to 6 GPa. The higher pressure melts also show decreasing Na/Ca and Al/Si in melts in equilibrium with garnet lherzolite, reflecting particularly an increase in the compatibility of Na_2O with respect to clinopyroxene, and decrease of compatibility of Al_2O_3 with respect to garnet. The experimental study by Tenner *et al.* (2012) on a lherzolite composition at 3·5 GPa, 1200–1450°C and bulk water contents of 1·5, 2·5 and 5 wt % yielded melt fractions of 18–33 modal % and a harzburgite (olivine > orthopyroxene) residue in most experiments. The disappearance of clinopyroxene followed by garnet as water content and melt fraction increase mirrors the predicted behaviour at 2·5 GPa illustrated in Fig. 5 (see also Supplementary Data EA 1). Melt compositions are olivine-rich, with high Ca/Al and low Na_2O contents, and in the one experiment with residual clinopyroxene, at 1350°C, 3·5 GPa, both melt and clinopyroxene have roughly half the Na_2O content of the melt and residual clinopyroxene in our experiment above the solidus at 1225°C, 4 GPa [i.e. consistent with the much higher inferred melt fraction in the Tenner *et al.* (2012) study]. Estimated water contents of the lowest temperature melts are 19–23 wt % H_2O (i.e. similar to our estimates). In both studies Na_2O is mildly incompatible with respect to clinopyroxene at 3·5–6 GPa, whereas it is strongly incompatible at 2·5 GPa (Supplementary Data Tables EA 4 and 5). In both studies the contamination by carbon influenced melt compositions, moving them towards high CaO and MgO and strongly silica-undersaturated compositions. Inadvertently, the contamination by small amounts of carbon is appropriate for application to both intraplate and MOR magmatism (e.g. Green & Falloon, 1998, 2005).

Although differing significantly in K_2O and Na_2O contents, and Na/Ca, reflecting the lower melt fraction and the lherzolite rather than harzburgite residue in our 4 and 6 GPa experiments, the normative compositions (Fig. 7) of the lowest temperature and most water-rich melts at 3·5 GPa in the study by Tenner *et al.* (2012) overlap with the 4 GPa, 1225°C, melt composition in this study. Similarly, the melt compositions at 3 GPa, 1375°C, ~5% H_2O (Balta *et al.*, 2011) and at 3 GPa, 1450°C, 'dry' (Davis *et al.*, 2011) are consistent with lower water contents and pressure differences (Fig. 7). As noted, the effects of carbon contamination in these studies are also identified as driving melt compositions towards more undersaturated and CaO-rich melts, and this is consistent with an essential role for both H_2O and CO_2 in the genesis of intraplate mantle-derived magmas.

Application to MORB petrogenesis

Primitive or parental MORB are characteristically depleted in large ion lithophile elements (LILE) and light rare earth elements (LREE), and the degree of relative depletion varies from low [normal (N)-MORB] to high [depleted (D)-MORB]. The water content in MORB glasses is correlated with Ce among the REE and also with K abundances (Danyushevsky *et al.*, 2000). Our study provides an explanation for these correlations in that estimates of the water content of source peridotite for N-MORB and D-MORB range from 100 to 250 ppm H_2O, a value within error of the water content retained in NAMs in residual fertile lherzolite after loss of hydrous silicate melt at the vapour-saturated solidus. Water contents and depletion in incompatible elements in the MORB-source result from loss of very small melt fraction(s) in the garnet lherzolite stability field. The lherzolitic source for N-MORB and D-MORB is envisaged as the deep levels of the asthenosphere (~7–8 GPa; Fig. 6), at levels that experience one or more (or 'continuous') extractions of extremely small melt fraction at or near the vapour (water)-saturated solidus. The process yields 'depleted but fertile' MORB-source lherzolite. The low water content of MORB-source lherzolite is not an indication of absence of melting but a consequence of incipient melting and loss of a near-solidus melt at the vapour-saturated solidus, leaving 'depleted' water and incompatible element contents in NAMs in the lower asthenosphere. This model of upwelling from the lower part of the asthenosphere can be further constrained by consideration of the temperatures of parental MORB and of inferred mantle potential temperature (T_p). From olivine and glass equilibrium relationships and examination of the most magnesian MORB glasses, it has been inferred that modern mantle acting as MORB sources has T_p ~1430°C (Green *et al.*, 2001, 2004; Falloon *et al.*, 2007*a*, 2007*b*) As the vapour-saturated solidus at >3 GPa has a greater dT/dP than the inferred mantle adiabat, a mantle adiabat with T_p ~1430°C is predicted to intersect with the vapour-saturated solidus at ~7–8 GPa (~230 to ~260 km, Fig. 6b).

The adiabatic upwelling of 'depleted but fertile' lherzolite from these depths to much shallower levels will yield higher melt fractions (~15–20% melt) matching parental MORB with ~0·1–0·2 wt % H_2O. The residual lherzolite to harzburgite will have <10 ppm H_2O, reflecting high temperatures of water partitioning and the very low water content of parental MORB (Hirth & Kohlstedt, 1996; Tenner *et al.*, 2009; Ardia *et al.*, 2012; Kovács *et al.*, 2012). As the depth of segregation of primitive MORB from residual lherzolite (i.e. the extraction of melt from a permeable flow regime or from an ascending diapir, and its movement to the surface in dykes or dunite channels) is at 1·5–2 GPa (Eggins, 1992*a*, 1992*b*; Green *et al.*, 2001, 2005; Falloon *et al.*, 2007*a*, 2007*b*), new residual lithosphere formed at this depth is 'dry' (as in Hirth & Kohlstedt, 1996). The establishment of the pargasite-controlled lithosphere–asthenosphere boundary (Green, 1971; Green & Liebermann, 1976; Green *et al.*, 2010, 2011) and thickening of the lithosphere with age are attributed to cooling and water access to the lithosphere as it moves away from the ridge setting.

Melting in the mantle wedge above subduction zones

Geophysical modelling of the subduction of ocean crust predicts distinctive inversion of T vs depth profiles in the mantle wedge above the seismic Benioff zone. Progressive dehydration of oceanic crust and uppermost mantle lithologies in the subducting slab causes release of water either as vapour (H_2O-dominated C–O–H–S vapour) or as water-rich silicate melt. There are many models of T distribution within the mantle wedge with diverse slab compositions, subduction rates and ages (temperatures) of subducted crust, dip of subducted slab and prehistory of the mantle wedge, all affecting estimates of T distribution. Accepting that the subduction process transports water into the mantle wedge, the experimentally determined phase relations for lherzolite + $H_2O \pm CO_2$ can be superimposed on these models and will predict regions of hydrous silicate melting and of carbonatite melting if CO_2 is present (Niida & Green, 1999; Tumiati *et al.*, 2013). This has been done previously using the phase relations for the model 'MOR-Pyrolite' composition (Green & Falloon, 1998; Niida & Green, 1999; Green *et al.*, 2004) and, given the close similarity of HZ1 and MOR-Pyrolite compositions, the detail of fig. 6 of Niida & Green (1999) is equally applicable to the HZ1 composition as a model composition in the mantle wedge setting. The significance of the depth interval near 80–100 km (i.e. P of 2·5–3 GPa) is emphasized as a 'step' or rapid change in the water-storage capacity of the mantle wedge lherzolite. Immediately above the slab and at shallower depths, water or hydrous silicate melt migrating up-temperature into the wedge from the slab can be 'captured' and stored (up to ~0·5 wt %; i.e. 20–30% pargasite) in fertile lherzolite below ~1100°C. Less modal pargasite and lower water storage capacity apply to more refractory lherzolite (Wallace & Green, 1991). Pargasite-bearing lherzolite formed at <100 km and dragged downward by the subducting slab will melt at ~100 km depth if its temperature is >1000°C, possibly initiating mantle upwelling and consequent magmatism. An important result from the present study is that because of the strongly positive dT/dP of the vapour-saturated solidus at >2·5 GPa and to 1375°C, 6 GPa, the modelled region of partial melting of (residual) lherzolite + (C, H, O) in the mantle wedge above the subduction zone is restricted to shallow depths in the subduction environment.

An additional conclusion from this study (see also Green *et al.*, 2010, 2011; Kovács *et al.*, 2012) is the recognition that if melting and melt extraction of lherzolite + (C, H, O) in subduction settings occurs at or near the vapour-saturated solidus (aqueous vapour) then the residue from such melting is not 'dry' and if carried deeper into the mantle will take up to ~200 ppm water with it into the deeper mantle. Also, subduction of intraplate lithosphere containing pargasite will lead to pargasite breakdown to NAMs + vapour ± phlogopite at the base and within the deeper parts of the slab, releasing >1000 ppm H_2O at ~3 GPa (Green, 1973*b*; Niida & Green, 1999; Green *et al.*, 2010, 2011) but ~150–200 ppm H_2O will remain for recycling into deeper mantle levels.

ACKNOWLEDGEMENTS

We thank Hugh O'Neill and Joerg Hermann for helpful discussions of the many facets of this study, particularly including the issues of supercritical fluids and water in NAMs. David Clark and Dean Scott provided technical assistance and maintained the high-pressure laboratory. S. Feig is thanked for assistance with use of the Hitachi FESEM at the Central Science Laboratory, University of Tasmania. R. W. Luth and S. Poli are thanked for comments on an earlier paper, and M. Wilson, R. W. Luth and anonymous reviewers are thanked for their editorial and reviewers' comments. D.H.G. thanks the School of Earth Sciences and Centre for Ore Deposit Studies at the University of Tasmania, and Research School of Earth Sciences at the Australian National University, for generous collegiality and access to research facilities as an honorary research associate.

FUNDING

This research was supported by Australian Research Council grants to D.H.G., and to G.M.Y. and D.H.G. I.K. was supported by an A. E. Ringwood Memorial Scholarship, an Australian International Postgraduate Research Scholarship, a Marie Curie International Reintegration Grant (NAMS-230937), a Bolyai Postdoctoral Fellowship Program, and a postdoctoral grant (PD101683) of the Hungarian Scientific Research

Fund. A.R. was supported by an ANU PhD Scholarship, an RSES 2007 joint 'Mervyn and Katalyn Paterson Fellowship', and a Marie Curie International Incoming Fellowship (302637).

SUPPLEMENTARY DATA

Supplementary data for this paper are available at *Journal of Petrology* online.

REFERENCES

Adam, J. (1988). Dry, hydrous and CO_2-bearing liquidus phase relationships in the CMAS system at 28 kb, and their bearing on the origin of alkali basalts. *Journal of Geology* **96**, 709–719.

Adam, J. (1990). The geochemistry and experimental petrology of sodic alkaline basalts from Oatlands, Tasmania. *Journal of Petrology* **31**, 1201–1223.

Adam, J., Green, T. H., Sie, S. H. & Ryan, C.G. (1997). Trace element partitioning between aqueous fluids, silicate melts and minerals. *European Journal of Mineralogy* **9**, 569–584.

Ardia, P., Hirschmann, M. M., Withers, A. C. & Tenner, T. J. (2012). H_2O storage capacity of olivine at 5–8 GPa and consequences for dehydration partial melting of the upper mantle. *Earth and Planetary Science Letters* **345–348**, 104–116.

Asimow, P. D., Dixon, J. E. & Langmuir, C. H. (2004). A hydrous melting and fractionation model for mid-ocean ridge basalts: Application to the Mid-Atlantic ridge near the Azores. *Geochemistry, Geophysics, Geosystems* **5**, Q01E16, doi:10.1029/2003GC000568.

Bali, E., Bolfan-Casanova, N. & Koga, K. T. (2008). Pressure and temperature dependence of H solubility in forsterite: an implication to water activity in the Earth interior. *Earth and Planetary Science Letters* **268**, 354–363.

Ballhaus, C. (1995). Is the upper mantle metal-saturated? *Earth and Planetary Science Letters* **132**, 75–86.

Ballhaus, C., Berry, R. F. & Green, D. H. (1990). Oxygen fugacity controls in the Earth's upper mantle. *Nature* **348**, 437–440.

Balta, J. B., Asimow, P. D. & Mosenfelder, J. L. (2011). Hydrous, low-carbon melting of garnet peridotite. *Journal of Petrology* **52**, 2079–2105.

Bonadiman, C., Coltorti, M., Comodi, P., Giuli, G. & Faccini, B. (2014). Crystal chemistry of amphiboles: implications for oxygen fugacity and water activity in lithospheric mantle beneath Victoria Land, Antarctica. *Contributions to Mineralogy and Petrology* **167(984).**

Bowen, N. L. & Tuttle, O. F. (1949). The system MgO–SiO_2–H_2O. *Geological Society of America Bulletin* **60**, 439–460.

Brey, G. & Green, D. H. (1975). The role of CO_2 in the genesis of olivine melilitite. *Contributions to Mineralogy and Petrology* **49**, 93–103.

Brey, G. & Green, D. H. (1977). Systematic study of liquidus phase relations in olivine melilitite + H_2O + CO_2 at high pressures and petrogenesis of an olivine melilitite magma. *Contributions to Mineralogy and Petrology* **61**, 141–162.

Danyushevsky, L. V., Eggins, S. M., Falloon, T. J. & Christie, D. M. (2000). H_2O abundance in depleted to moderately enriched mid-ocean ridge magmas: Part I: incompatible behaviour, implications for mantle storage, and origin of regional variations. *Journal of Petrology* **41**, 1329–1364.

Dasgupta, R. & Hirschmann, M. M. (2006). Melting in the Earth's deep upper mantle caused by carbon dioxide. *Nature* **440**, 659–662.

Dasgupta, R., Mallik, A., Tsuno, K., Withers, A., Hirth, G. & Hirschmann, M. M. (2013). Carbon-dioxide-rich silicate melt in the Earth's upper mantle. *Nature* **493**, 211–215.

Davis, F. A., Hirschmann, M. M. & Humayun, M. (2011). The composition of the incipient partial melt of garnet peridotite at 3 GPa and the origin of OIB. *Earth and Planetary Science Letters* **308**, 380–390.

Dixon, J. E. & Clague, D. A. (2001). Volatiles in basaltic glasses from Loihi seamount, Hawaii: Evidence for a relatively dry plume component. *Journal of Petrology* **42**, 627–654.

Edgar, A. D., Green, D. H. & Hibberson, W. O. (1976). Experimental petrology of a highly potassic magma. *Journal of Petrology* **17(3)**, 339–356.

Eggins, S. M. (1992*a*). Petrogenesis of Hawaiian tholeiites: 1. Phase equilibria constraints. *Contributions to Mineralogy and Petrology* **110**, 387–397.

Eggins, S. M. (1992*b*). Petrogenesis of Hawaiian tholeiites: 2. Aspects of dynamic melt segregation. *Contributions to Mineralogy and Petrology* **110**, 398–410.

Falloon, T. J. & Danyushevsky, L. D. (2000). Melting of refractory mantle at 1·5, 2 and 2·5 GPa under anhydrous and H_2O-undersaturated conditions: implications for the petrogenesis of high-Ca boninites and the influence of subduction components on mantle melting. *Journal of Petrology* **41**, 257–283.

Falloon, T. J. & Green, D. H. (1988). Anhydrous partial melting of peridotite from 8 to 35 kb and the petrogenesis of MORB. *Journal of Petrology*, Special Lithosphere Issue, 379–414.

Falloon, T. J. & Green, D. H. (1989). The solidus of carbonated, fertile peridotite. *Earth and Planetary Science Letters* **94**, 364–370.

Falloon, T. J. & Green, D. H. (1990). Solidus of carbonated fertile peridotite under fluid-saturated conditions. *Geology* **18**, 195–199.

Falloon, T. J., Danyushevsky, L. V., Ariskin, A. & Green, D. H. (2007*a*). The application of olivine geothermometry to infer crystallization temperatures of parental liquids: implications for the temperature of MORB magmas. *Chemical Geology* **241**, 207–233.

Falloon, T. J., Green, D. H. & Danyushevsky, L. V. (2007*b*). Crystallization temperatures of tholeiite parental liquids: implications for the existence of thermally driven mantle plumes. In: Foulger, G. R. & Jurdy, D. M. (eds) *The Origins of Melting Anomalies: Plates, Plumes, and Planetary Processes. Geological Society of America, Special Papers* **430**, 235–260.

Faul, U. H. & Jackson, I. N. S. (2007). Diffusion creep of dry, melt-free olivine. *Journal of Geophysical Research* **112**, B04204, doi:10.1029/2006JB004586(2007).

Fei, H. Z., Wiedenbeck, M., Yamazaki, D. & Katsura, T. (2013). Small effect of water on upper-mantle rheology based on silicon self-diffusion coefficients. *Nature* **498(7453)**, 213–215.

Fischer, K. M., Ford, H. A., Abt, D. L. & Rychert, C. A. (2010). The lithosphere–asthenosphere boundary. *Annual Review of Earth and Planetary Sciences* **38**, 551–575.

Foley, S. F. (1989). The genesis of lamproitic magmas in a reduced, fluorine-rich mantle. In: Ross, J. (ed.) *Kimberlites and Related Rocks*. Melbourne: Blackwell, pp. 616–631.

Foley, S. F. (2011). A reappraisal of redox melting in the Earth's mantle as a function of tectonic setting and time. *Journal of Petrology* **52(7–8)**, 1363–1391.

Foley, S. F., Yaxley, G. M., Rosenthal, A., Buhre, S., Kiseeva, E. S., Rapp, R. P. & Jacob, D. E. (2009). The composition of near-solidus melts of peridotite in the presence of CO_2 and H_2O between 40 and 60 kbar. *Lithos* **112**, Part 1, Special Issue S1, 274–283.

Frey, F. A., Green, D. H. & Roy, S. D. (1978). Integrated models of basalt petrogenesis—a study of quartz tholeiites to olivine

melilitites from southeastern Australia utilizing geochemical and experimental petrological data. *Journal of Petrology* **19**, 463–513.

Frost, D. J. & McCammon, C. A. (2008). The redox state of Earth's mantle. *Annual Review of Earth and Planetary Sciences* **36**, 389–420.

Fumagalli, P., Zanchetta, S. & Poli, S. (2009). Alkali in phlogopite and amphibole and their effects on phase relations in metasomatized peridotite: a high pressure study. *Contributions to Mineralogy and Petrology* **158**, 723–737.

Gaetani, G. A., O'Leary, J. A., Koga, K. T., Hauri, E. H., Rose-Koga, E. F. & Monteleone, B. D. (2014). Hydration of mantle olivine under variable water and oxygen fugacity conditions. *Contributions to Mineralogy and Petrology* **167**, 965.

Gaillard, F., Malki, M., Iacono-Marziano, G., Pichavant, M. & Scaillet, B. (2008). Carbonatite melts and electrical conductivity in the asthenosphere. *Science* **322**, 1363–1365.

Girard, J., Chen, J., Raterron, P. & Holyoke, C. W. (2013). Hydrolytic weakening of olivine at mantle pressure: Evidence of [100](010) slip system softening from single-crystal deformation experiments. *Physics of the Earth and Planetary Interiors* **216**, 12–20.

Green, D. H. (1971). Composition of basaltic magmas as indicators of conditions of origin: application to oceanic volcanism. *Philosophical Transactions of the Royal Society of London, Series A* **268**, 707–725.

Green, D. H. (1972). Contrasted melting relations in a pyrolite upper mantle under mid-ocean ridge, stable crust and island arc environments. *Tectonophysics* **17(3)**, 285–297.

Green, D. H. (1973*a*). Conditions of melting of basanite magma from garnet peridotite. *Earth and Planetary Science Letters* **17**, 456–465.

Green, D. H. (1973*b*). Experimental melting studies on a model upper mantle composition at high pressures under water-saturated and water-undersaturated conditions. *Earth and Planetary Science Letters* **19**, 37–53.

Green, D. H. (1976). Experimental testing of 'equilibrium' partial melting of peridotite under water-saturated, high-pressure conditions. *Canadian Mineralogist* **14**, 255–268.

Green, D. H. & Falloon, T. J. (1998). Pyrolite: a Ringwood concept and its current expression. In: Jackson, I. (ed.) *The Earth's Mantle*. Cambridge: Cambridge University Press, pp. 311–378.

Green, D. H. & Falloon, T. J. (2005). Primary magmas at mid-ocean ridges, 'hotspots', and other intraplate settings: Constraints on mantle potential temperature. In: Foulger, G. R., Natland, J. H., Presnall, D. C. & Anderson, D. L. (eds) *Plates, Plumes, and Paradigms*. *Geological Society of America, Special Papers* **388**, 217–247.

Green, D. H. & Hibberson, W. (1970). Experimental duplication of conditions and precipitation of high pressure phenocrysts in a basaltic magma. *Physics of the Earth and Planetary Interiors* **3**, 247–254.

Green, D. H. & Liebermann, R. C. (1976). Phase equilibria and elastic properties of a pyrolite model for the oceanic upper mantle. *Tectonophysics* **32**, 61–92.

Green, D. H. & Ringwood, A. E. (1967). The genesis of basaltic magmas. *Contributions to Mineralogy and Petrology* **15**, 103–190.

Green, D. H. & Wallace, M. E. (1988). Mantle metasomatism by ephemeral carbonatite melts. *Nature* **336**, 459–462.

Green, D. H., Nicholls, I., Viljoen, M. & Viljoen, R. (1975). Experimental demonstration of the existence of peridotitic liquids in the earliest Archean magmatism. *Geology* **3**, 11–14.

Green, D. H., Falloon, T. J. & Taylor, W. R. (1987). Mantle-derived magmas: roles of variable source peridotite and variable C–H–O fluid compositions. In: Mysen, B. O. (ed.) *Magmatic Processes: Physicochemical Principles*. Washington, DC: Geochemical Society, pp. 139–154.

Green, D. H., Falloon, T. J., Eggins, S. M. & Yaxley, G. M. (2001). Primary magmas and mantle temperatures. *European Journal of Mineralogy* **13(3)**, 437–451.

Green, D. H., Schmidt, M. & Hibberson, W. O. (2004). Island-arc ankaramites: primitive melts from fluxed refractory lherzolitic mantle. *Journal of Petrology* **45(2)**, 391–403.

Green, D. H., Hibberson, W. O., Kovács, I. & Rosenthal, A. (2010). Water and its influence on the lithosphere–asthenosphere boundary. *Nature* **467**, 448–451.

Green, D. H., Hibberson, W. O., Kovács, I. & Rosenthal, A. (2011). Water and its influence on the lithosphere–asthenosphere boundary (vol. 467, 448–451, 2010). [Addendum.]. *Nature* **472(7344)**, 504.

Green, D. H., Rosenthal, A. & Kovács, I. (2012). Comment on 'The beginnings of hydrous mantle wedge melting', CB Till, TL Grove, AC Withers. *Contributions to Mineralogy and Petrology* **164(6)**, 1077–1081.

Grove, T. L., Chatterjee, N., Parman, S. W. & Medard, E. (2006). The influence of H_2O on mantle wedge melting. *Earth and Planetary Science Letters* **249**, 74–89.

Gudmundsson, G. & Wood, B. J. (1995). Experimental tests of garnet peridotite oxygen barometry. *Contributions to Mineralogy and Petrology* **119**, 56–67.

Hall, L. J., Brodie, J., Wood, B. J. & Carrol, M. R. (2004). Iron and water losses from hydrous basalts contained in $Au_{80}Pd_{20}$ capsules at high pressure and temperature. *Mineralogical Magazine* **68**, 1, 75–81.

Hart, S. R. & Zindler, A. (1986). In search of a bulk-Earth composition. *Chemical Geology* **57**, 247–267.

Hauri, E. H., Gaetani, G. A. & Green, T. H. (2006). Partitioning of water during melting of the Earth's upper mantle at H_2O-undersaturated conditions. *Earth and Planetary Science Letters* **248**, 715–734.

Hirano, N., Takahashi, E., Yamamoto, J., Abe, N., Ingle, S. P., Kaneoka, I., Hirata, T., Kimura, J. I., Ishii, T., Ogawa, Y., Machida, S. & Suyehiro, K. (2006). Volcanism in response to plate flexure. *Science* **313**, 1426–1428, doi:10.1126/science.1128235.

Hirschmann, M. M. (2006). Water, melting, and the deep Earth H_2O cycle. *Annual Review of Earth and Planetary Sciences* **34**, 629–653.

Hirschmann, M. M., Tenner, T. J., Aubaud, C. & Withers, A. C. (2009). Dehydration melting of nominally anhydrous mantle: The primacy of partitioning. *Physics of the Earth and Planetary Interiors* **176**, 54–68.

Hirth, G. & Kohlstedt, D. L. (1996). Water in the oceanic upper mantle: implications for rheology, melt extraction and the evolution of the lithosphere. *Earth and Planetary Science Letters* **144**, 93–108.

Irving, A. J. & Green, D. H. (2008). Phase relationships of hydrous alkalic magmas at high pressures: Production of nepheline hawaiitic to mugearitic liquids by amphibole-dominated fractional crystallization within the lithospheric mantle. *Journal of Petrology* **49(4)**, 741–756.

Katz, R. F., Spiegelman, M. & Langmuir, C. H. (2003). A new parameterization of hydrous mantle melting. *Geochemistry, Geophysics, Geosystems* **4(9)**, 1073, doi:10.1029/2002GC000433.

Kind, R., Yuan, X. & Kumar, P. (2012). Seismic receiver functions and the lithosphere–asthenosphere boundary. *Tectonophysics* **536**, 25–43.

Konzett, J. & Ulmer, P. (1999). The stability of hydrous potassic phases in lherzolitic mantle—an experimental study to 9·5 GPa in simplified and natural bulk compositions. *Journal of Petrology* **40**, 629–652.

Kovács, I., Hermann, J., O'Neill, H. St. C., FitzGerald, J. D., Sambridge, M. & Horvath, G. (2008). Quantitative absorbance spectroscopy with unpolarized light, Part II: Experimental evaluation and development of a protocol for quantitative analysis of mineral IR spectra. *American Mineralogist* **93**, 765–778.

Kovács, I., Green, D. H., Rosenthal, A., Hermann, J., O'Neill, H. St. C., Hibberson, W. O. & Udvardi, B. (2012). An experimental study of water in nominally anhydrous minerals in the upper mantle near the water-saturated solidus. *Journal of Petrology* **53**, 2067–2093.

Kushiro, I., Syono, Y. & Akimoto, S. (1968). Melting of a peridotite nodule at high pressures and high water pressures. *Journal of Geophysical Research* **73**, 6023–6029.

Lambert, I. B. & Wyllie, P. J. (1970). Melting in the deep crust and upper mantle and the nature of the low velocity layer. *Physics of the Earth and Planetary Interiors* **3**, 316–322.

Medard, E. & Grove, T. L. (2008). The effect of H_2O on the olivine liquidus of basaltic melts: experiments and thermodynamic models. *Contributions to Mineralogy and Petrology* **155**, 417–432.

Mengel, K. & Green, D. H. (1989). Stability of amphibole and phlogopite in metasomatized peridotite under water-saturated and water-undersaturated conditions. In: Ross, J. (ed.) *Kimberlites and Related Rocks, Vol. 1, Their Composition, Occurrence, Origin and Emplacement. Geological Society of Australia, Special Publication* **14**, 571–581.

Mibe, K., Fujii, T. & Yasuda, A. (2002). Composition of aqueous fluid coexisting with mantle minerals at high pressure and its bearing on the differentiation of the Earth's mantle. *Geochimica et Cosmochimica Acta* **66**, 2273–2285.

Mibe, K., Kanzaki, M., Kawamoto, T., Matsukage, K. N., Fei, Y. & Ono, S. (2007). Second critical endpoint in the peridotite–H_2O system. *Journal of Geophysical Research* **112**, B03201, doi:10.1029/2005JB004125.

Michael, P. J. (1995). Regionally distinctive sources of depleted MORB: evidence from trace elements and H_2O. *Earth and Planetary Science Letters* **131**, 301–320.

Millhollen, G., Irving, A. J. & Wyllie, P. J. (1974). Melting interval of peridotite with 5·7 per cent water to 30 kilobars. *Journal of Geology* **82**, 575–587.

Mysen, B. & Boettcher, A. L. (1975). Melting of a hydrous mantle: Parts I and II. Phase relations of a natural peridotite at high pressures and temperatures with controlled activities of water, carbon dioxide, and hydrogen. *Journal of Petrology* **16(3)**, 520–593.

Nakamura, Y. & Kushiro, I. (1974). Composition of the gas phase in Mg_2SiO_4–SiO_2–H_2O at 15 kbar. *Carnegie Institution of Washington Yearbook* **73**, 255–258.

Nicholls, I. & Ringwood, A. E. (1973). Effect of water on olivine stability in tholeiites and the production of silica-saturated magmas in the island-arc environment. *Journal of Geology* **81**, 285–300.

Niida, K. & Green, D. H. (1999). Stability and chemical composition of pargasitic amphibole in MORB pyrolite under upper mantle conditions. *Contributions to Mineralogy and Petrology* **135**, 18–40.

Niu, Y. L. & O'Hara, M. J. (2009). MORB mantle hosts the missing Eu (Sr, Nb, Ta and Ti) in the continental crust: New perspectives on crustal growth, crust–mantle differentiation and chemical structure of oceanic upper mantle. *Lithos* **112**, 1–17.

Odling, N. W. A., Green, D. H. & Harte, B. (1997). The determination of partial melt compositions of peridotite systems by melt inclusion synthesis. *Contributions to Mineralogy and Petrology* **129**, 209–221.

O'Neill, H. St. C. & Wall, V. J. (1987). The olivine–orthopyroxene–spinel oxygen geobarometer, the nickel precipitation curve, and the oxygen fugacity of the Earth's upper mantle. *Journal of Petrology* **28**, 1169–1191.

O'Neill, H. St. C., Rubie, D. C., Canil, D. *et al.* (1993). Ferric iron in the upper mantle and in transition zone assemblages: implications for relative oxygen fugacities in the mantle. In: Takahashi, E., Jeanloz, R. & Rubie, D. C. (eds) *Evolution of the Earth and Planets. American Geophysical Union, Geophysical Monograph* **74**, 73–88.

Rohrbach, A. & Schmidt, M. W. (2011). Redox freezing and melting in the Earth's deep mantle resulting from carbon–iron redox coupling. *Nature* **472**, 209–212.

Rohrbach, A., Ballhaus, C., Golla-Schindler, U., Ulmer, P., Kamenetsky, V. S. & Kuzmin, D. V. (2007). Metal saturation in the upper mantle. *Nature* **449**, 456–458.

Rosenthal, A., Yaxley, G. M., Green, D. H., Hermann, J., Kovács, I. & Spandler, C. (2014). Continuous eclogite melting and variable refertilisation in upwelling heterogeneous mantle. *Scientific Reports* **4**, 6099, doi: 10.1038/srep06099.

Rychert, C. A. & Shearer, P. M. (2011). Imaging the lithosphere–asthenosphere boundary beneath the Pacific using SS waveform modeling. *Journal of Geophysical Research* **116**, B07307, doi:10.1029/2010JB008070.

Saal, A. E., Hauri, E. H., Langmuir, C. H. & Perfit, M. R. (2002). Vapour undersaturation in primitive mid-ocean ridge basalt and the volatile content of Earth's upper mantle. *Nature* **419**, 451–455.

Schmerr, N. (2012). The Gutenberg discontinuity: melt at the lithosphere–asthenosphere boundary. *Science* **335**, 1480–1483.

Scott, J. M., Hodgkinson, A., Palin, J. M., Waight, T. E., Van der Meer, Q. H. A. & Cooper, A. F. (2014). Ancient melt depletion overprinted by young carbonatitic metasomatism in the New Zealand lithospheric mantle. *Contributions to Mineralogy and Petrology* **167(1)**, 963.

Sifré, D., Gardés, E., Massuyeau, M., Hashim, L., Hier-Majumder, S. & Gaillard, F. (2014). The electrical conductivity during incipient melting in the oceanic low velocity zone. *Nature* **509(7498)**, 81–85.

Spandler, C., Yaxley, G. M., Green, D. H. & Scott, D. (2010). Experimental phase and melting relations of metapelite in the upper mantle: implications for the petrogenesis of intraplate magmas. *Contributions to Mineralogy and Petrology* **160**, 569–589.

Stagno, V. & Frost, D. J. (2010). Carbon speciation in the asthenosphere: experimental measurements of the redox conditions at which carbonate-bearing melts coexist with graphite or diamond in peridotite assemblages. *Earth and Planetary Science Letters* **300**, 72–84.

Stagno, V., Ojwang, D. O., McCammon, C. A. & Frost, D. J. (2013). The oxidation state of the mantle and the extraction of carbon from Earth's interior. *Nature* **493**, 84–88.

Stalder, R. (2012). Comment on 'The beginnings of hydrous mantle wedge melting', CB Till, TL Grove, AC Withers. *Contributions to Mineralogy and Petrology* **164(6)**, 1077–1081.

Stalder, R., Ulmer, P., Thompson, A. B. & Gunther, D. (2001). High pressure fluids in the system MgO–SiO_2–H_2O under upper mantle conditions. *Contributions to Mineralogy and Petrology* **140**, 607–618.

Taylor, W. R. (1985). The role of C–O–H fluids in upper mantle processes—a theoretical, experimental and spectroscopic study, PhD thesis, University of Tasmania, Hobart.

Taylor, W. R. & Green, D. H. (1988). Measurements of reduced peridotite–C–O–H solidus and implications for redox melting of the mantle. *Nature* **332**, 349–352.

Tenner, T. J., Hirschmann, M. M., Withers, A. C. & Hervig, R. L. (2009). Hydrogen partitioning between nominally anhydrous upper mantle minerals and melt between 3 and 5 GPa and applications to hydrous peridotite partial melting. *Chemical Geology* **262(1–2)**, 42–56.

Tenner, T. J., Hirschmann, M. M. & Humayun, M. (2012). The effect of H_2O on partial melting of garnet peridotite at 3·5 GPa. *Geochemistry, Geophysics, Geosystems* **13**, doi:10.1029/2011GC003942.

Thibault, Y., Edgar, A. D. & Lloyd, F. E. (1992). Experimental investigation of melts from a carbonated phlogopite lherzolite: implications for metasomatism in the continental lithosphere. *American Mineralogist* **77**, 784–794.

Thybo, H. (2006). The heterogeneous upper mantle low velocity zone. *Tectonophysics* **416(1–2)**, 53–79.

Thybo, H. & Perchuc, E. (1997). The seismic 8° discontinuity and partial melt in the continental mantle. *Science* **275**, 1626–1629, doi:10.1126/science.275.5306.1626.

Till, C. B., Grove, T. L. & Withers, A.C. (2012*a*). The beginnings of hydrous mantle wedge melting. *Contributions to Mineralogy and Petrology* **163(4)**, 669–688.

Till, C. B., Grove, T. L. & Withers, A. C. (2012*b*). Reply to 'Comment on "The beginnings of hydrous mantle wedge melting" by Till *et al.*' by Green, Rosenthal and Kovacs. *Contributions to Mineralogy and Petrology* **164(6)**, 1083–1085.

Tumiati, S., Fumagalli, P., Tinaboschi, C. & Poli, S. (2013). An experimental study on COH-bearing peridotite up to 3·2 GPa, and implications for crust–mantle recycling. *Journal of Petrology* **54**, 453–479.

Wallace, M. E. & Green, D. H. (1988). An experimental determination of primary carbonatite magma composition. *Nature* **335**, 343–346.

Wallace, M. E. & Green, D. H. (1991). The effect of bulk rock composition on the stability of amphibole in the upper mantle: implications for solidus positions and mantle metasomatism. *Mineralogy and Petrology* **44**, 1–19.

Wendlandt, R. & Eggler, D. H. (1980). The origins of potassic magmas: 2. Stability of phlogopite in natural spinel lherzolite and in the system $KAlSiO_4$–MgO–SiO_2–H_2O–CO_2 at high pressures and high temperatures. *American Journal of Science* **280**, 421–458.

Wyllie, P. J. (1978). Mantle fluid compositions buffered in peridotite–CO_2–H_2O by carbonates, amphibole, and phlogopite. *Journal of Geology* **86(6)**, 687–713.

Wyllie, P. J. (1979). Magmas and volatile components. *American Mineralogist* **64**, 469–500.

Wyllie, P. J., Huang, W.-L., Otto, J. & Byrnes, A. P. (1983). Carbonation of peridotites and decarbonation of siliceous dolomites represented in the system CaO–MgO–SiO_2–CO_2 to 30 kbar. *Tectonophysics* **100**, 359–388.

Yaxley, G. M. & Green, D. H. (1996). Experimental reconstruction of sodic dolomitic carbonatite melts from metasomatised lithosphere. *Contributions to Mineralogy and Petrology* **124**, 359–369.